IMPROVING THE PIEZOELECTRIC PROPERTIES OF FLEXIBLE POLYMER-NANOPARTICLE ENERGY HARVESTERS

by

Muhammet Emin Cavusoglu

A Thesis

Submitted to the
Department of Mechanical Engineering
In partial fulfillment of the requirement
For the degree of
Master of Science in Mechanical Engineering
at
Rowan University
May 18, 2020

Thesis Advisor: Wei Xue, Ph.D.

Dedications

I would like to dedicate my work to my mother, father, and my older brother, Zülal, Nejdet, and Bülent Cavusoglu, who have given me strength and provided moral, emotional, and spiritual support during this not only wonderful but also challenging journey. I also would like to dedicate my work to Emrah Yetimoglu who financially supported me along this journey.

Acknowledgments

First and foremost, I would like to express my deep and sincere gratitude to my research supervisor Dr. Wei Xue. He has taught me everything I needed to take this research from beginning to the finish line. His sincerity, enthusiasm, vision, and encouragement have profoundly motivated and inspired me. It was an enormous honor to work under his guidance. I would also like to express my thanks to Dr. Francis Haas and Dr. Smitesh Bakrania for being a part of my defense committee.

I would also like to extend my thanks to my brilliant and exceptional lab mates and my dear friends, Rhandy Paladines, Harrison Hones, Jordan Cook, Muhammad Usman, and Gregg Murray for their support, ideas and their friendship. I would also like to thank my roommates, Emre Bal, Seifuldin Elsherbiny, and Ahmed Ahsour for their support and truthful friendship.

I also like to thank all the people who have supported me directly and indirectly along this journey.

Abstract

Muhammet Emin Cavusoglu
IMPROVING THE PIEZOELECTRIC PROPERTIES OF FLEXIBLE POLYMER-NANOPARTICLE ENERGY HARVESTERS
2018-2020
Wei Xue, Ph.D.
Master of Science in Mechanical Engineering

In this research, one of the widely used polymers, poly(vinylidene fluoride) (PVDF), was used to develop thin-film polymer energy harvesters. Dimethylformamide (DMF) and methyl ethyl ketone (MEK) were used to dissolve the PVDF powder. Four different (0%, 3%, 5%, and 7%) ZnO nanoparticle (NP) concentrations were used to enhance the electrical output of the thin-film energy harvesters. A sonication bath and additional MEK were used in dispersing the ZnO NPs to obtained uniform PVDF/ZnO NP solution. The electrode poling technique was used for dipole alignment to improve the electrical performance of the devices. The fabricated samples were tested using the tensile testing method to investigate the mechanical properties of thin-film energy harvesters for each ZnO NP concentrations. PVDF thin-film samples with 7% ZnO NPs had the lowest Young's modulus at 994.21 MPa. The voltage and power output of fabricated devices were increased as a result of embedding ZnO NPs and polarization. The highest power and peak-to-peak output voltage were produced by poled PVDF thin-film energy harvester with 7% ZnO NPs. The harvested power value was 31.14 mW which was 94% higher than the unpoled pure PVDF thin-film devices; the highest peak-to-peak voltage was measured as 11.2 V which was 84% higher than that of the unpoled pure PVDF thin-film devices.

Table of Contents

Table of Contents (Continued)

List of Figures

Figure Page

List of Figures (Continued)

Figure Page

List of Figures (Continued)

Figure Page

List of Tables

Table Page

Chapter 1

Introduction

1.1 Energy Harvesting

In the energy generation process for energy provision, non-renewable sources, such as oil, coal, natural gas, have been used for decades and the demand for energy has been increasing day by day. However, fossil fuels will run out quickly, they are expensive and limited, also they have damaging pollution effects. It is therefore essential to develop new energy sources that are renewable or sustainable. There are different forms of energy sources besides fossil fuels, such as mechanical energy, solar energy, geothermal energy, bio-energy, wind power, nuclear energy, etc., in our environment that can be utilized [1]. Alternative energy sources could be one of the solutions for climate change.

Portable low-power electronic devices are used in every part of our daily lives as a result of the rapid development of technology. In other words, technology has reached a point where we can make practical and useful systems down to the milliwatts (mW) or even lower range. However, portable low-power devices require batteries in order to function. As it is known that batteries contain several hazardous metals such as lead and mercury. Used batteries harm the environment because of these highly toxic metals and other chemicals. Therefore, in the last few decades scientists have been working on the idea how to make these portable devices self-powered [2, 3]. This is where energy harvesting becomes important.

The purpose of energy harvesting is to capture and convert the energy from external or ambient sources, such as radio frequency (RF), solar, flow, vibration, human

movements, etc., into electrical energy that can be used to power low-energy electronics, such as medical implants, wireless sensor networks, and wearable devices [4, 5]. Thus, it becomes possible to harvest useful energy out of the environment using energy harvesting technology for macro- and micro-electronic devices. Among all the renewable energy sources, the mechanical energy from human movements, such as walking, running, heartbeat, and touching, or vibration from the environment, is a widely available energy sources in nature. Therefore, piezoelectric and triboelectric energy harvesters or nanogenerators (NGs), which can convert mechanical energy into electrical energy, have been intensively studied. One interesting aspect of energy harvesting is that the generated energy needs to be stored temporarily for future long-term use. This technology might make low-energy electronics to have an infinite life span (energy-wise) by making it possible to charge these devices while using them [6]. For instance, a pacemaker needs to be replaced every 5-7 years due to the low battery issue. Combining this energy harvesting technology with pacemakers would make it possible to charge their batteries by the muscle movements of patients. This would save patients from multiple surgeries and extra costs in order to change their pacemakers.

1.2 Triboelectric Effect

The triboelectric effect is that certain materials become electrically charged when they are in contact with other materials through friction [7]. When two triboelectric materials make a physical contact, opposite static charges come into existence. This phenomenon happens between the triboelectric layers during the process of touching and separation [8]. As a result, an electric current starts to flow between the electrodes which are connected to these two triboelectric layers. A common example that most people have

seen is the phenomenon that when a rubber balloon is rubbed against hair, then put the balloon on the wall, the balloon would stick to the wall. It is because the balloon gets charged by the triboelectric effect. Another example is that sometimes we get an electric shock when we touched a car's door, especially in winters. Thus, it can be said that most of the static electricity is triboelectricity. It mostly happens in winter because static electricity appears easily when the temperature is cold, and the air is dry. In other words, as moisture in air can help dissipate electrons, the lack of it in cold, dry air during winter results in accumulated electrons on insulating surfaces.

The use of triboelectric effect in energy harvesting was first invented by Wang et al. in 2012 [9]. After their discovery, the attention on this promising technology has rapidly increased, for example, in 2012 the number of publications related to triboelectric nanogenerators (TENGs) was six, and this number reached up to 444 publications in 2018 [10].

Figure 1 shows four fundamental models for TENGs that include vertical contact-separation mode, in-plane sliding mode, single-electrode mode, and free-standing triboelectric-layer mode [11, 12]. Vertical contact-separation mode (a) is that when two materials have physical contact and separation movements, the motion creates electrical charges in opposite signs on the surfaces of the materials. If these materials are connected to electrodes, once the separation starts, the gap will cause a potential difference between the electrodes. If the device is connected to an external load, an electric current will start flowing in the circuit as a result of the potential drop.

The in-plane sliding mode can be seen in Figure 1b. In the same manner as the contact-separation mode when two triboelectric materials have physical contact, surface

charge transfer appears due to the triboelectric effect. Here the difference is that instead of having a full separation between the two triboelectric materials, the sliding back and forth between these two materials in the parallel direction using external force causes a partial displacement. Therefore, if these two materials are connected to electrodes, a potential difference is generated.

Single-electrode mode (Figure 1c) as is evident from its name, only one electrode is used when two electrodes are used for contact-separation mode and in-plane sliding mode. Having two electrodes connected to each other comes with a limitation. In other words, those systems are not applicable when the triboelectric effect needs to be used to generate electricity from freely moving objects. Thus, this is where the single-electrode method becomes important. In this method, one of the triboelectric materials is connected to the ground with an electrode and the other triboelectric material can move freely. Before the separation stage, these two materials are in full contact. With the help of the electrode, the electrons will flow from the ground to the material when the negatively charged material separates. When the connection between these two materials happens again, electrons will flow from the material to the ground because of the increment of positive charges. Electricity will be generated when this full separation and connection cycle is completed.

For the freestanding triboelectric-layer mode, as seen in Figure 1d, two triboelectric layers, which are connected to each other by an electrode, are needed underneath a dielectric layer. Also, there should be a gap between these two triboelectric layers. Electricity is generated due to the back and forth movement of the dielectric layer.

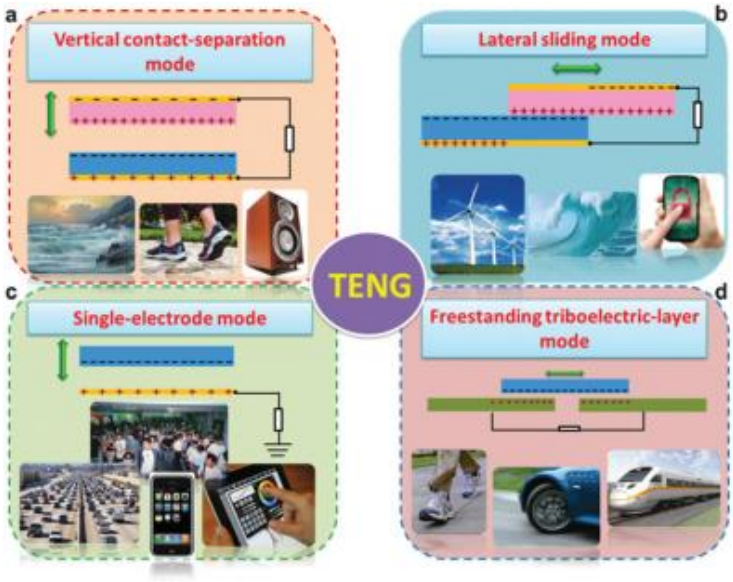

Figure 1. Fundamental models for TENGs: a) Vertical contact-separation mode. b) In-plane sliding mode. c) Single-electrode mode. d) Free-standing triboelectric-layer mode [11, 12].

1.3 Piezoelectric Effect

The word “piezoelectric” comes from the Greek word “piezein”, which means to squeeze or press [13]. The piezoelectric effect was first discovered by Pierre Curie and his brother Jacques Curie in 1880 [14]. They discovered that if they compressed certain crystals, positive and negative charges would appear on opposite sides. This difference in charges meant that the compressed crystals could drive an electric current through a circuit, which is defined as direct piezoelectric effect (Figure 2a). On the other hand, running electricity through these crystals makes them change their shapes, which is defined as converse piezoelectric effect (Figure 2b).

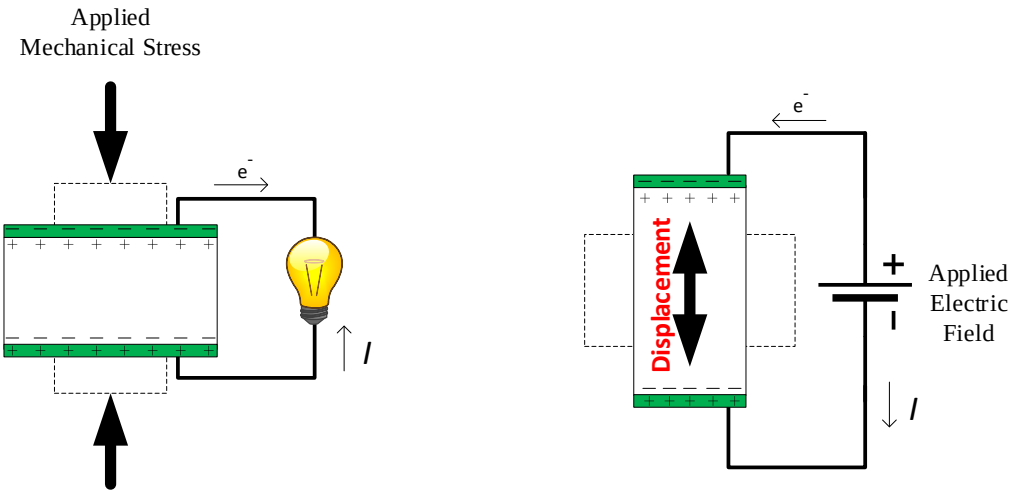

a) Direct piezoelectric effect ***b)*** Converse piezoelectric effect

Figure 2. a) Direct piezo effect: a voltage is generated when mechanical stress is applied on a piezoelectric material. b) Converse piezo effect: the shape of a piezoelectric material is changed under an applied electric field.

The general principle of converting mechanical energy into electrical energy using piezoelectric materials is shown in Figure 3. Basically, capturing the mechanical stress happens in Step-I, converting the captured mechanical stress into electrical energy happens in Step-II, then the processing and storing the generated electrical output by using a rectifier and an AC-DC converter circuit happen in Step-III [15-17].

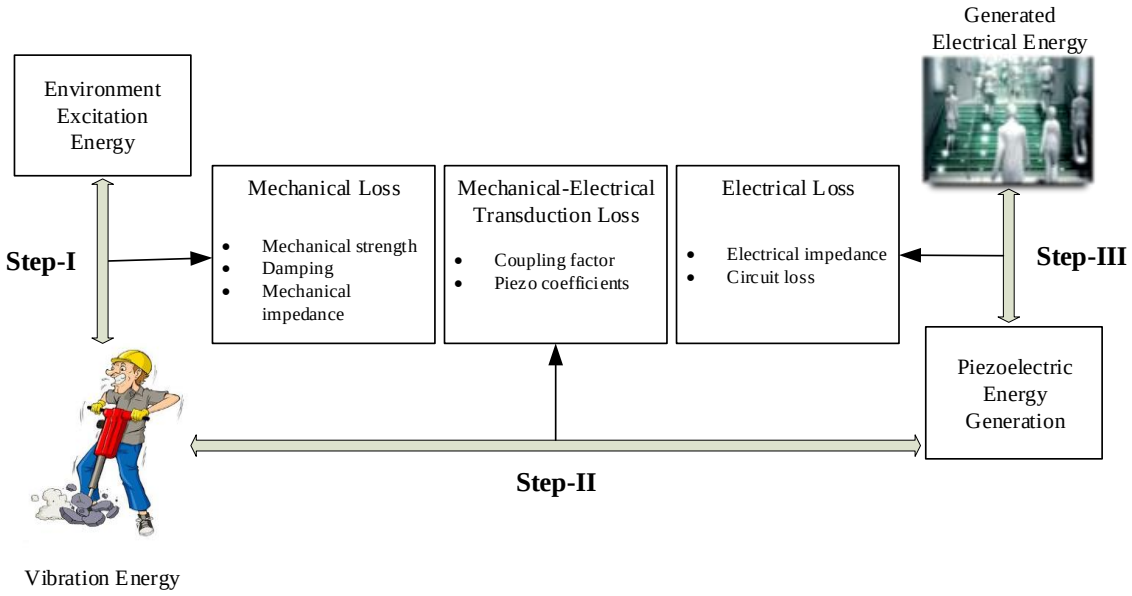

Figure 3. Energy flow of piezoelectric generators.

A better understanding of piezoelectric effect requires a close examination of the material's atomic structures [18]. Many materials are made of atoms which are arranged in an orderly three-dimensional pattern and distributed symmetrically. That pattern has a unit cell, and it repeats itself over and over again along the three dimensions in the material (Figure 4). Some crystalline materials do not have a center of symmetry, which makes these materials promising candidates for piezoelectric applications. However, this condition is not enough for these materials to exhibit piezoelectricity. They also need to have ionic or partially ionic bonds.

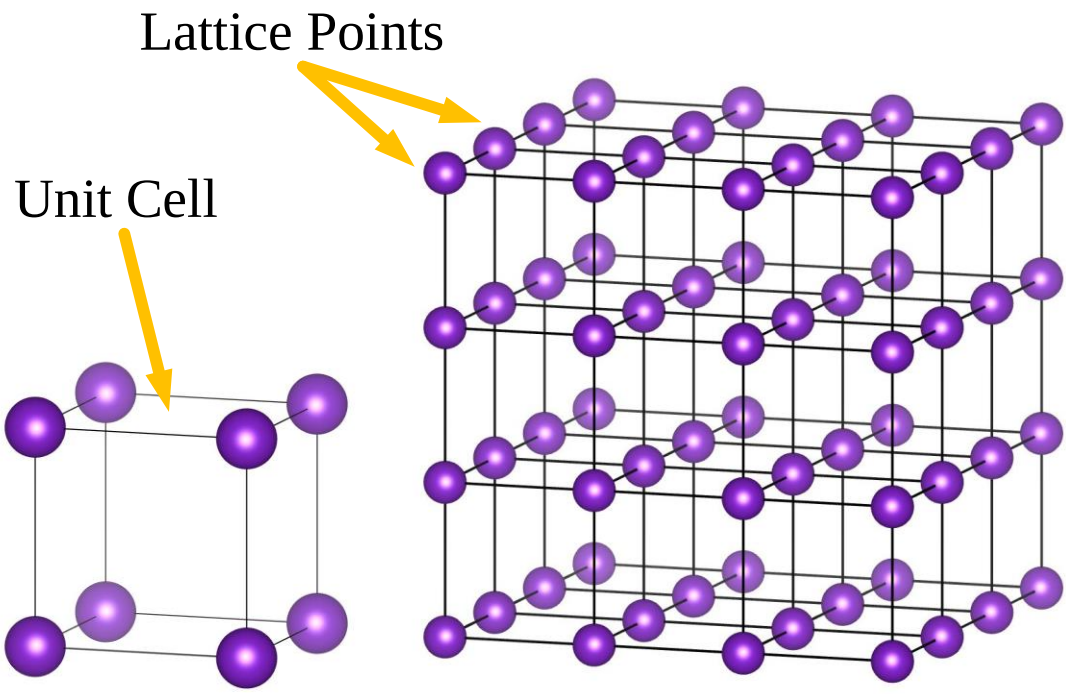

Figure 4. A unit cell shows the locations of lattice points repeating in all directions (metal).

For instance, the lattice structure of quartz (SiO_2) is made of silicon and oxygen in a hexagonal shape (Figure 5). In an un-compressed crystal, the negative and positive charges have a spatial arrangement without a net charge distribution (red). When this hexagonal shape is under tension, the two side negative charges move outwards, but the top negative charge moves downwards, thus the average position of these three negative charges move downwards (yellow). Also, the two side positive charges move outwards, but the bottom positive charge moves upwards, thus the average position of these three negative charges move upwards (blue). This means that squeezing quartz in a specific orientation shift all the positive charges in one direction and all the negative charges in

the other directions. The crystal under compression shows the opposite effect in terms of charge generation.

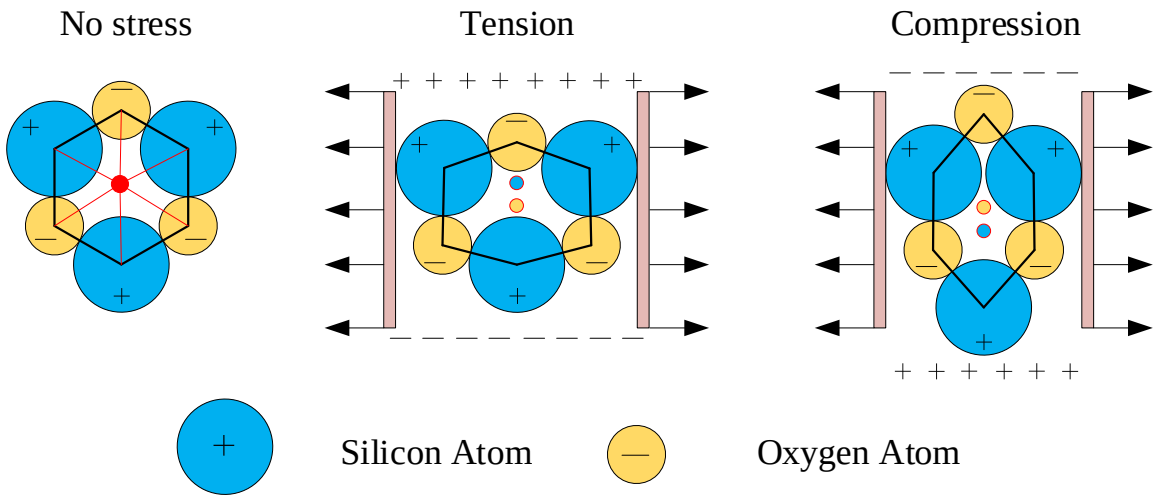

Figure 5. Piezoelectric effect in quartz.

1.3.1 Piezoelectric coefficients. Another important fundamental concept to understand the piezoelectric effect is piezoelectric material constant, which indicates the interaction between the mechanical and electrical behavior of a material. In addition, piezoelectric materials are anisotropic which makes their properties direction dependent [19]. Since piezoelectric outputs depend on the direction of the applied strain (S), stress (T) and electric field (E), defining these directions, or axes, has become essential. The x, y, and z axes are defined as directions 1, 2, and 3, respectively, and the rational axes around x, y, and z are represented by 4, 5, and 6, respectively (Figure 6). These axes with numbers help define the directions of mechanical stress or strain as well as the electric field.

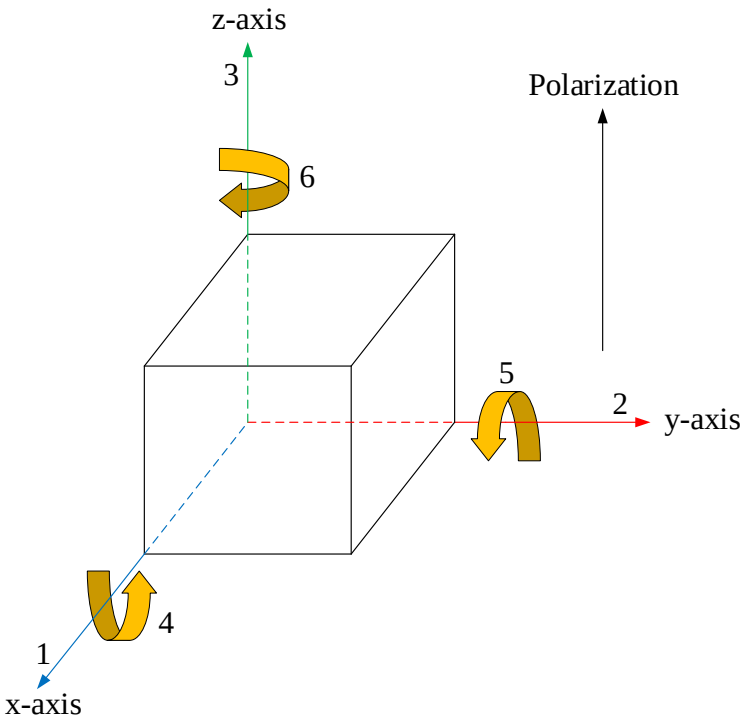

Figure 6. Notation of crystal axes with polarization direction in piezoelectric materials.

In order to show how active a piezoelectric material is and the level of interaction between its mechanical and electrical quantities, piezoelectric constants with two subscripts are identified using these directions and numbers. There are two commonly used piezoelectric constants (Table 1): piezoelectric charge constant, d_{ij}, with the applied stress in *j*-axis and the generated electric field in *i*-axis, and piezoelectric voltage constant, g_{ij}, with the strain produced in *j*-axis and the applied electric field in *i*-axis. The two most common operation modes for piezoelectric materials are 31 and 33 modes. The performance of piezoelectric devices highly depends on the directions of both applied stress and electric field. For instance, the d_{33} mode coefficient of lead zirconate titanate (PZT), one of the most common piezoelectric materials, is almost two times higher than

the coefficient d_{31}, 225 pC/N and 110 pC/N, respectively. As a result, the voltage output generated in the d_{33} mode is expected to be greater than that in the d_{31} mode [1, 20].

Table 1

Piezoelectric constants and two common modes (31 and 33)

d_{33} (C/N)	The applied stress in 3-axis and generated electric field in 3-axis.
d_{31} (C/N)	The applied stress in 1-axis and generated electric field in 3-axis.
g_{33} (m^2/C)	The strain produced in 3-axis and the applied electric field in 3-axis.
g_{31} (m^2/C)	The strain produced in 1-axis and the applied electric field in 3-axis.

In addition, there is a correlation between piezoelectric charge constant and piezoelectric voltage constant (equation 1). Having high piezoelectric charge constant and piezoelectric voltage constant value results high piezoelectric performance [21].

$$g = \frac{d}{\varepsilon} \quad (1)$$

ε: Permittivity.

1.4 Piezoelectric Materials

There are numerous natural materials that have piezoelectric properties. These materials can be seen in Figure 7. However, most of these materials do not show sufficient piezoelectric properties for practical applications. Consequently, synthetic piezoelectric materials have been produced.

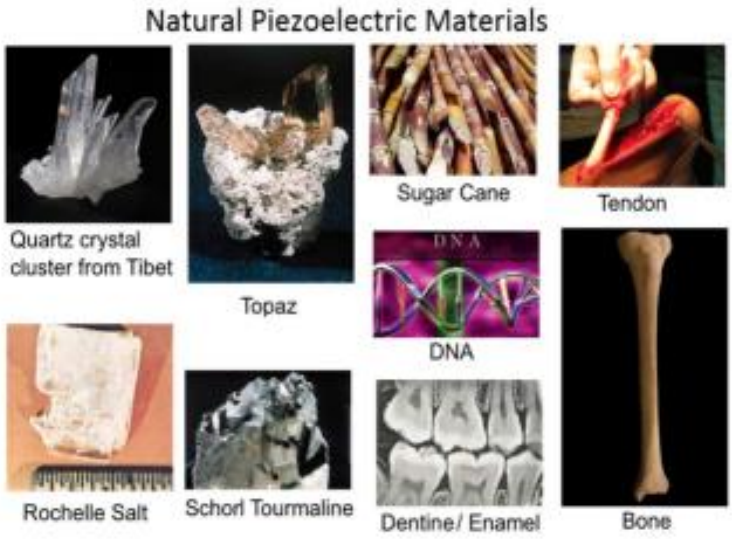

Figure 7. Natural piezoelectric materials [22].

After the discovery of the piezoelectric effect in 1880 by the Curie brothers, piezoelectric materials did not draw enough attention for practical applications until World War I. The first practical application of piezoelectricity was in sonar instruments to detect German submarines during World War I by Paul Langevin and his colleagues [23]. After World War I, in 1921, a very important discovery of ferroelectricity in the crystal of Rochelle salt was made by Joseph Valasek [24]. In 1935, the piezoelectric effect in potassium dihydrogen phosphate (KDP) was discovered by Busch and Scherrer [25]. Nevertheless, these materials were not suitable for practical applications due to their low Curie temperatures [26]. Barium titanate ($BaTiO_3$) was the first discovered material to have applicable ferroelectric properties with a perovskite structure by two different and independent scientists group in Russia and the U.S.A., in 1945 and 1946, respectively [26].

Jaffe and his colleagues discovered the PZT family of ceramics with promising piezoelectric properties in 1954 [27]. After decades of research and development, $BaTiO_3$ and PZT still attract considerable attention of researchers in this field. However, piezoelectric ceramics are not flexible enough to be used for complicated shapes and they require high processing temperatures [28]. On the other hand, piezoelectric polymers such as poly(vinylidene fluoride) (PVDF) and its co-polymer poly(vinylidene fluoride-trifluoroethylene) (PVDF-TrFE) can be used for complex shapes due to its flexibility at low temperature. They also have other unique advantages such as easy processing, low manufacturing cost, and high compatibility with biological applications [29].

1.4.1 Piezoelectric ceramics. Piezoelectric ceramics are used in a number of applications such as medical devices (ultrasonic equipment and fetal health monitors), automotive components (seat belt and tire pressure sensors), computer equipment (inject printers), etc. Among all piezoelectric ceramics, PZT, BaTiO3, and ZnO are the most extensively used piezo ceramic materials for applications in NGs and self-powered sensors [29].

1.4.1.1 Lead zirconate titanate (PZT). PZT based ceramics have been studied by scientists since its discovery. It is one of the most popular piezoelectric ceramics due to their low manufacturing costs, impressive dielectric and piezoelectric response, and mechanical properties [30]. For example, its piezoelectric charge coefficient is d33 ~ 250–600 pC/N and Curie temperature is Tc ~ > 300°C [31]. PZT is a synthetic material and its general chemical formula is Pb[ZrxTi1−x]O3 ($0 \leq x \leq 1$) [22, 29, 32]. Its chemical structure can be seen in Figure 8. Applying external forces such as pressure, electric field,

or heating to move the zirconium (Zr) atom, which is in the center position of PZT's unit cell, causes a charge deflection, resulting in generated electricity in PZT [22].

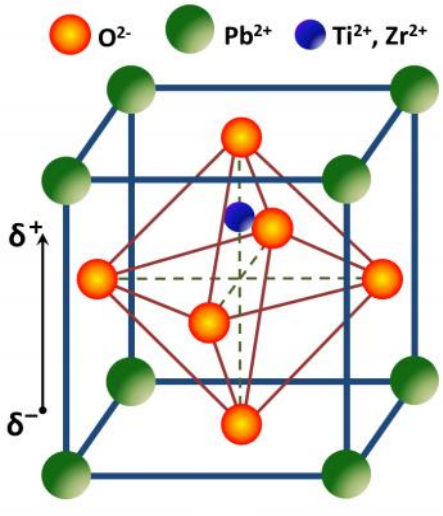

Figure 8. A unit cell structure of PZT ceramic under an electric field [22].

PZT films are key elements in piezoelectric and pyroelectric sensors, nonvolatile memory elements, photoelectric devices, energy harvesting devices, and actuators [33-36]. However, PZT loses its piezoelectric properties over its Curie temperature, T_c, and its operating temperature is typically limited at 150°C [36-38]. Another disadvantage of PZT based ceramics is their low biocompatibility due to the toxic effect of lead (Pb) elements that have harmful effects on the environment and human bodies, such as brain and nervous system [39, 40]. Therefore, it is hard to use this material for practical applications, such as aerospace, wearable, and biomedical devices.

1.4.1.2 Lead-free piezoelectric materials: $BaTiO_3$ and ZnO. Lead-containing piezoelectric ceramics had been widely studied and used in different industries until the European Union introduced the new restrictions on using lead-containing and toxic materials in commercial products in 2002 [41]. This new regulation had raised a significant need and interest in high performance lead-free piezoelectric materials which can be comparable to PZT based ceramics.

$BaTiO_3$ (BT) was the first discovered polycrystalline ferroelectric material, even before PZT based piezo ceramics [41]. Despite their low Curie temperatures $T_c \sim < 100°C$ and low depolarization temperatures (T_d), $BaTiO_3$ based lead-free piezoelectric materials have promising properties, such as easy processing, as well as impressive electrical and mechanical properties [31, 42]. However, its piezoelectric properties are still lower than PZT based ceramics.

ZnO nanoparticles (NPs) have also attracted a lot of attention due to their piezoelectric properties, large surface area, strong voltage, stable chemical properties, and different bond states inside the nanoparticles and on the surface as well [43, 44]. Although its piezoelectric properties are not at the desired level comparing to piezoelectric properties of PZT based ceramics.

Under the circumstances that are mentioned above, neither $BaTiO_3$ nor ZnO is a great material to replace PZT. However, it is quite hard to avoid their piezoelectric properties. Therefore, these materials can be used as fillers to help improving piezoelectric output. Considering all these reasons, ZnO nanoparticles were chosen as our filler to improve the piezoelectric output of our samples.

1.4.2 Piezoelectric polymers. Piezoelectric polymers are lightweight, flexible, and non-toxic while piezo-ceramics are toxic, brittle, and heavy [29, 39, 45, 46]. There are basically three different piezo-polymers categories which are bulk piezoelectric polymers, voided charged polymers, and piezoelectric polymer composites (Figure 9) [29, 47, 48].

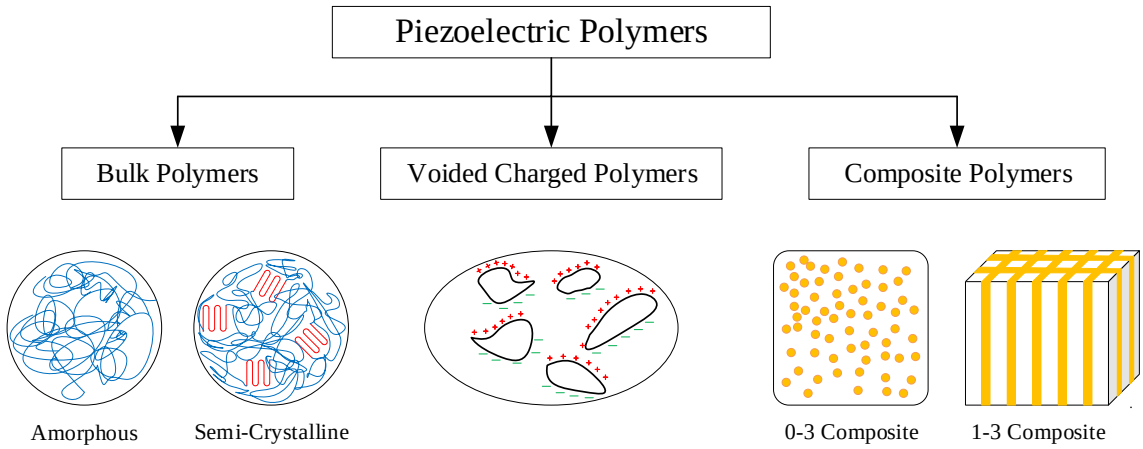

Figure 9. Classification and structural details of piezoelectric polymers: bulk piezo polymers, voided charged polymers, and piezoelectric polymer composites.

Bulk polymers have piezoelectric properties because of their molecular structure and orientation. Also, they are classified into two groups which are amorphous and semi-crystalline polymers due to their molecular structures [29, 47]. Voided charged polymers, also known as ferroelectrets, are polymer foams and their structures are filled with gas molecules such as air [49]. These gas molecules play important roles to speed up the opposite charges when an electric field is applied. Piezoelectric composites are the combination of polymers and inorganic materials or nanoparticles which have

piezoelectric properties [15, 50]. Moreover, these polymers are important for wearable and flexible electronics applications since ceramic piezoelectric materials are not suited for these applications.

1.4.2.1 Poly(vinylidene fluoride) [PVDF]. Piezoelectric properties in a polymer, PVDF, were discovered for the first time by Kawai in 1969 [51]. Ever since, PVDF and its copolymers have been heavily investigated due to their promising piezoelectric properties, easy processing for complex shapes, low manufacturing cost, and biocompatibility [29, 52]. Piezoelectric polymers have been used for many different applications such as actuators, tactile devices, energy conversion, medical devices, etc. [53].

PVDF is a semi-crystalline polymer and it has five crystalline phases, α, β, γ, δ, and ε [54, 55]. The non-polar α-phase (Figure 10a) with trans-gauche-trans-gauche conformation (TGTG') and the polar β-phases (Figure 10b) with all-trans conformation (TTT) are the two most common, also the most studied, phases in PVDF [56, 57]. Moreover, the β-phase is the most important phase because of its piezoelectric, pyroelectric and ferroelectric properties due to its highest dipole moment per unit cell, 8×10^{-30} Cm, among all crystalline phases of PVDF [15, 55, 58]. The γ-phase is not as a common phase as α and β-phases because it is a transitional phase between α and β-phases [54, 59]. Chemical structure of PVDF can be seen in Figure 10c.

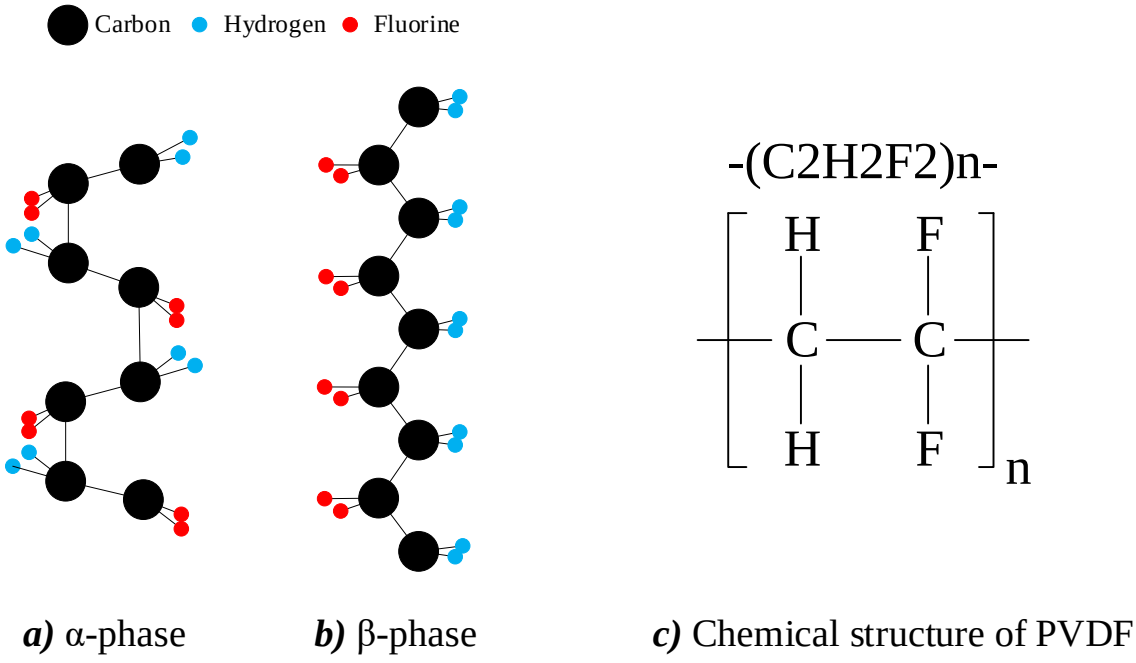

Figure 10. a) α-phase (TGTG' configuration) and b) β -phase (TTT configuration) of PVDF. c) Chemical structure of PVDF. Elements present: carbon, hydrogen, fluorine.

PVDF has five crystalline phases, α, β, γ, δ, and ε [54, 55]. A more detailed expilanation for these crystalline phases will be covered later in this thesis. β-phase is the most important one in this field. One of the criteria that makes β-phase important is that the piezoelectric properties of a material depend on its polar crystalline structure [15, 60]. The all-trans conformation (TTT) structure in the β-phase makes PVDF to have more dipole alignment which gives PVDF strong piezoelectricity [61]. Therefore, obtaining a higher β-phase content in PVDF could help improve its piezoelectric response.

Table 2 illustrates important physical and piezoelectric properties of three materials (PZT, PVDF, and $BaTiO_3$). Among them, PVDF is the most flexible material that makes it a better choice for complex designs. Also, the density of PVDF is lower

than that of PZT and $BaTiO_3$, approximately four times and three times lower, respectively. Moreover, since PVDF is a non-toxic material, which makes it a good candidate for medical and wearable applications such as peacemaker, despite its low Curie temperature and piezoelectricity. However, the low piezoelectricity of PVDF can be enhanced by embedding piezo-nanoparticles, dipoles arrangement, etc.

Table 2

Comparing important physical and piezoelectric parameters for PZT, PVDF and BaTiO3 [15, 18, 62, 63]

Properties	Units	PZT	PVDF	$BaTiO_3$
Piezoelectricity	-	High	Low	Good
Mechanical flexibility	-	Poor	Excellent	Good
Biocompatibility	-	Poor	Good	Good
Dielectric constant ($\varepsilon/\varepsilon_0$)		1200	12	1700
Piezo-strain constant	10^{-12} C/N	d_{31}=110, d_{33}=225-590	d_{31}=8-23, d_{33}=-34	d_{31}=-78 d_{33}=190
Piezo-stress constant	10^{-3} V m/N	g_{31}=10, g_{33}=26	g_{31}=216, g_{33}=-330	g_{31}=5, g_{33}=11.4
Curie temperature	°C	386	80	115-130
Density	10^3 kg/m^3	7.5	1.78	5.7

Considering all these factors, PVDF was the chosen polymer for this project. In later chapters, a detailed explanation about fabrication, enhancement of electrical and

mechanical properties, and testing methods for this polymer will be discussed in this thesis.

1.4.2.2 Poly(vinylidene fluoride-trifluoroethylene) [PVDF-TrFE]. PVDF-TrFE was first discovered by Tamemoto in 1979 [64]. PVDF-TrFE is a copolymer of PVDF with additional trifluoroethylene (TrFE) units. Studies have shown that integrating TrFE improved the crystal properties of PVDF [65]. Moreover, the chain conformation of PVDF from the non-polar α-phase to the polar β-phase has become possible without applying secondary treatment such as electrode poling [64, 66]. In other words, the trifluoroethylene in PVDF blocks the C-C chains in the non-polar conformation (TGTG') and allows more β-phase contents with all-trans chain conformation (TTT) [65]. Since the β-phase is of the primary interest for piezoelectricity, PVDF-TrFE has better piezo-electric, dielectric, and electrical properties than PVDF [66]. Besides its high piezoelectric response, PVDF-TrFE has high chemical and thermal stability [67]. Furthermore, PVDF-TrFE has better crystallinity than PVDF with higher polarization [47]. Its general molecular formula is (C2H2F2)a(C2HF2)b and the chemical structure of PVDF-TrFE can be seen in Figure 11.

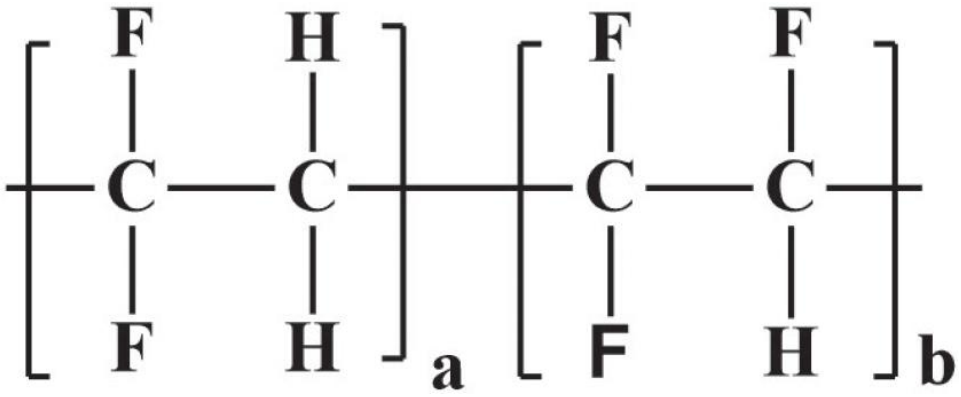

Figure 11. Chemical structure of PVDF-TrFE [15].

1.5 Piezoelectric Polymers Based Energy Harvesters

Polymer based energy generators have been studied over the past 20 years. There are different fabrication methods to process piezoelectric polymers such as spin coating, electrospinning, sol-gel method, etc. Also, there are different fillers, especially nano fillers, to improve the output of energy harvesters.

Research has shown that embedding additional ZnO nano fillers into piezo-polymers (PVDF or PVDF-TrFE) can enhance the electrical properties of these polymers due to the interfacial interaction between nanoparticles and polymers [68]. There are different types of ZnO nano fillers such as ZnO nanoparticles, nanorods, nanotubes, nanofibers, and nanowires [43]. For instance, in 2014, Zhang et al. [69] made PVDF-ZnO nanowires hybrid generators and improved the β-phase content and stability of the PVDF nanogenerators. In 2011, Dodds et al. [70] embedded different amounts of ZnO NPs to enhance the piezoelectricity of PVDF-TrFE bulk thin-films. In 2015, Bafqi et al. [71] have reported that integrating ZnO into PVDF can improve the β-phase and electrical response of PVDF samples. In 2019, Han et al. [43] investigated PVDF-TrFE thin-films by integrating different amounts of ZnO NPs . This study showed that decreasing the size

of ZnO NPs could increase the energy storage of piezoelectric thin-films due to small size ZnO NPs have a large surface area. Another observation from this study was that increasing the amount of ZnO NPs could affect the quality of thin-films. Moreover, enhanced voltage output was observed when the amount of ZnO was less than 10%.

In 2014, Hartono et al. [72] investigated the poling technique's effect on PVDF piezo polymers at different temperatures. It demonstrated that electrode poling increased the β-phase of the polymer with enhanced piezoelectric properties [73, 74].

In 2013, another study presented by Mahadeva et al. [75] demonstrated that the poling effect, based on corona poling, depends on different poling time and voltages Figure 12a shows how the β-phase content could change depending on the poling time. Moreover, significant voltage output improvement after the poling process can be seen in Figure 12b-c. For example, under a 3 N force the voltage output is around 0.13 V before poling, and under the same force it is around 5.5 V after poling.

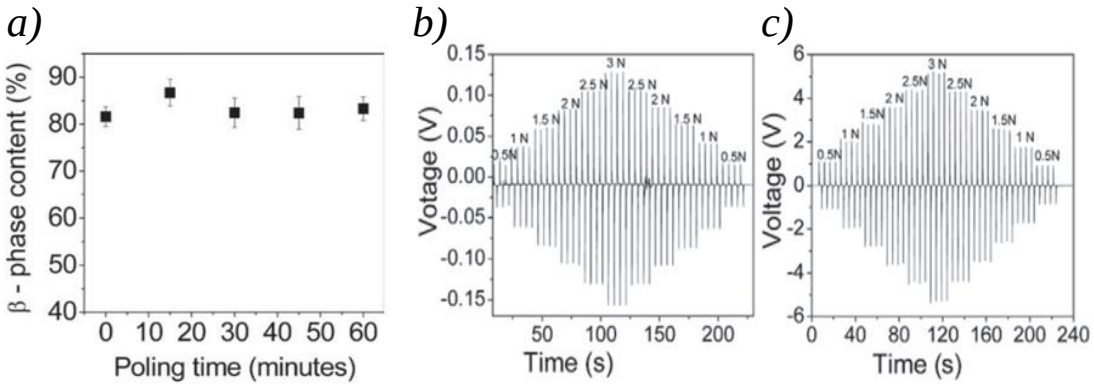

Figure 12. a) Impact of poling time on the β-phase content of a PVDF sample (T=80°C). b) Voltage output measurement of an unpoled PVDF sample and c) poled PVDF sample at 80°C for 45 min [75].

1.6 Applications

In 2019, Dong et al. [76] intended to develop a PVDF-TrFE thin-film piezoelectric nanogenerator, which can be placed between a pacemaker and human cardiovascular system to charge the battery of the peacemaker by converting the bending energy of the pacemaker to electrical energy. Energy consumption of a pacemaker is approximately 0.78 µW per day and this device can produce 0.9 µW energy per day under laboratory conditions. The results showed that this energy harvesting device could help recharge the batteries in the traditional cardiac pacemakers and eliminate unnecessary periodic surgeries for replacement pacemakers.

In 2016, Nour et al. [77] embedded ZnO nanowires into PVDF-TrFE and fabricated a nanogenerator that could convert the mechanical energy from human footsteps into electrical energy for self-powered pressure sensors with future applications in wireless sensor networks. Figure 13 demonstrates that the average voltage output and the functionality of the device via LED display by foot pressing.

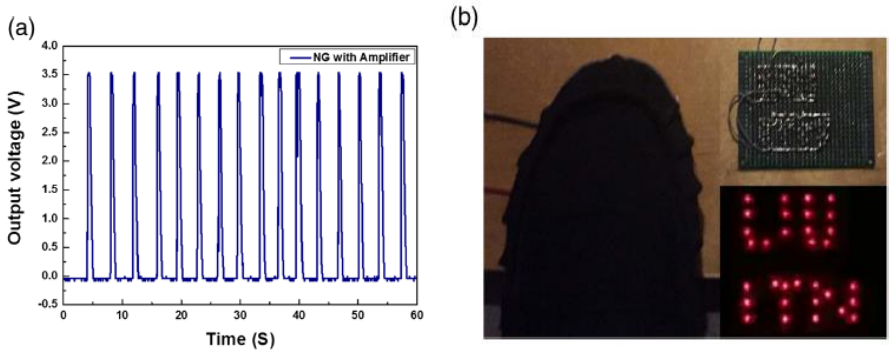

Figure 13. a) The average output voltage. b) The energy-harvesting circuits connected to LED display triggered by foot pressing [77].

1.7 Motivation and Objectives

Finding new ways to generate renewable, sustainable, and eco-friendly energy has become essential due to the global warming and the energy crisis around the world. There are various energy forms, such as solar energy, mechanical energy, wind power, etc. to harvest energy besides fossil fuels. Among all these energy sources, harvesting energy from the wasted mechanical energy in the environment has attracted enormous attention because it is environmentally friendly and easily available. Piezoelectric polymers have been widely used to develop eco-friendly and non-toxic devices to capture mechanical energy from the environment and convert into electrical energy. However, it is still challenging to develop efficient devices for that purpose. Thus, this research aims to investigate pure PVDF and PVDF composites with different ZnO NP concentrations to obtain high performance, flexible, and biocompatible thin-film energy harvesters to power macro- and micro-electronic devices. The project is designed to explore the relationship between the integrated ZnO NPs as fillers and the electrical properties of thin-film energy harvesters as well as their mechanical properties. Moreover, the project aims to investigate the impact of electrode poling on the piezoelectric properties of PVDF thin-film energy harvesters.

The objectives of this research include;

1. Develop high-quality PVDF thin-film composites embedding different ZnO NP concentrations to capture human based mechanical energy from the environment.
2. Investigate mechanical properties of PVDF thin-film energy harvesters.

3. Observe the effect of electrode poling method and integrating various ratios of ZnO NPs on electrical properties of polymer based thin-film energy harvesters.

Chapter 2

Fabrication of Energy Harvester Thin-Films Devices

The raw PVDF material needs to be processed before it can be used for energy harvesting applications. The flow chart of the fabrication process can be seen in Figure 14. The fabrication process starts with dissolving the PVDF powder in a solvent on a hot plate using the magnetic stirring technique. The second step is mixing the PVDF solution with ZnO NPs in a glass vial and placing it in a sonication bath. After obtaining a uniform PDVF/ZnO NPs solution, the solvent is evaporated using a hot plate, and then, a vacuum desiccator is used to remove air bubbles from the solution. The next step is to spin coat the solution on a glass slide to acquire thin-film samples. The fabrication process ends with placing the glass slides on a hot plate for annealing.

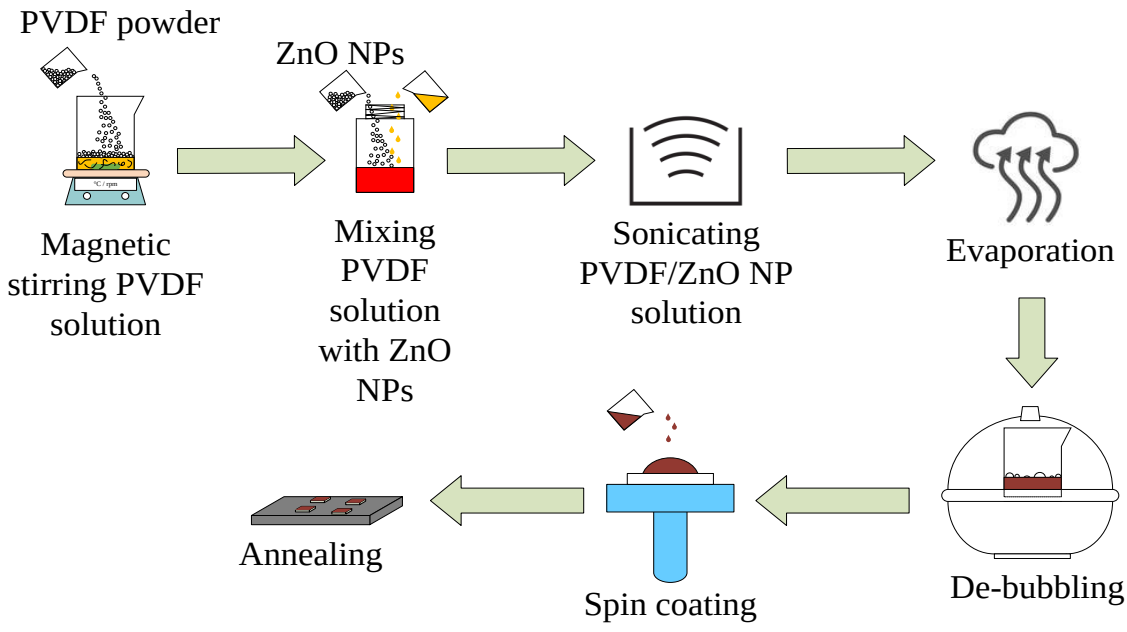

Figure 14. Flow chart for fabrication process of the PVDF/ZnO NPs thin-film energy harvesters.

2.1 Materials and Solvents

2.1.1 Piezoelectric polymer (PVDF). PVDF is the most commonly used polymer for piezoelectric applications due to its various properties, as previously described [29, 52]. PVDF has been used for many different applications such as energy harvesting, actuators, sensing, tactile devices, biomedical fields, etc. [29, 47, 56, 78].

The melting point of PVDF is 167°C. Above 150°C the γ-phase is the dominant phase in PVDF and below this temperature the α-phase is dominant [61, 74]. There are a number of methods to obtain these phases depends on the processing methods in deposition and thermal processes [52]. Some of these methods and criteria to obtain the β-phase in PVDF are shown in Table 3. The first column illustrates different steps, such as annealing at high pressure, drawing at high temperature, and poling at high electric field, to transform α-phase to β-phase. Drawing at the temperature below 100°C causes the transformation from α-phase to β-phase [73, 74]. It has also been observed that between 70-100°C, both α and β-phases may be present [74]. Thus, the β-phase has appeared to be most stable when the temperature is between 70-90°C. Another important method to make the transformation from α-phase to β-phase is poling the sample at high electric field in order to achieve desired dipolar alignment. The β-phase also could be obtained from the γ-phase by poling the PVDF thin-film energy harvesters at high electric field and temperature (above 120°C). The δ-phase can be transformed into β-phase by poling at high electric field.

Table 3

Transformation methods to obtain the β-phase from α, γ, and δ-phases

	from α-phase to β-phase	from γ-phase to β-phase	from δ -phase to β-phase
Annealing at high pressure (P)	✓	✓	X
Ultra-drawing at high temp (T)	✓	X	X
Drawing at low temp (T)	✓	X	X
Poling at high electric field (E)	✓	X	✓

The PVDF powder used in this research was purchased from Sigma-Aldrich (molecular weight: 530,000, density (ρ): 1.74 g/mL at 25 °C, melting temperature: 171°C). Figure 15 shows an example of the PVDF powder used in our experiments.

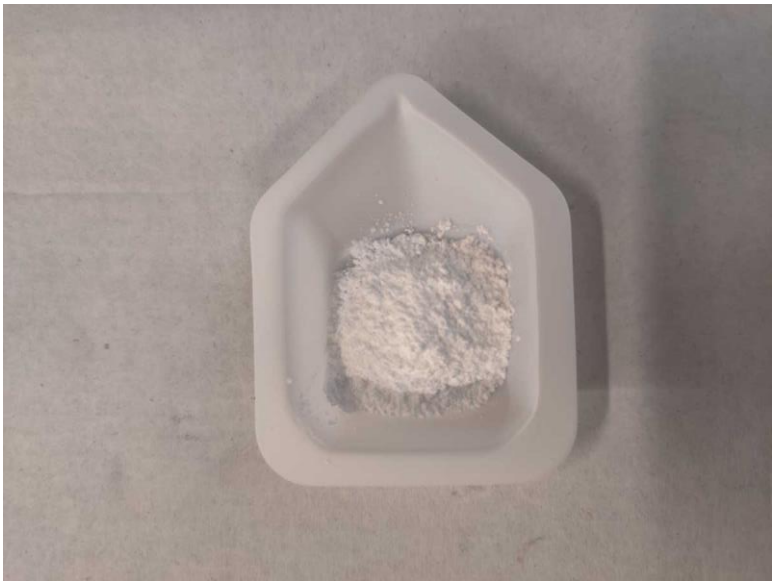

Figure 15. Powder PVDF used in our experiments.

2.1.2 ZnO nanoparticles. There are a number of differently shaped ZnO nanomaterials such as nanorods, nanoplates, nanowires, nanoparticles, etc. [79]. Even for nanoparticles alone, there are different sizes of ZnO NPs from commercial vendors with their diameters up to 200 nm. Figure 16 shows the ZnO NPs used in this study. They were purchased from Nanoamore, with a 99.5% purity and an average diameter of 20 nm. ZnO NPs are important for this research due to their piezoelectric properties, semi-conductivity and biocompatibility [43, 44]. Moreover, the nanostructure of ZnO can be deformed even under very small mechanical stresses [80]. Integrating different concentrations of ZnO NPs with PVDF enhances the output of energy harvesting devices [70], which will be discussed later in this thesis.

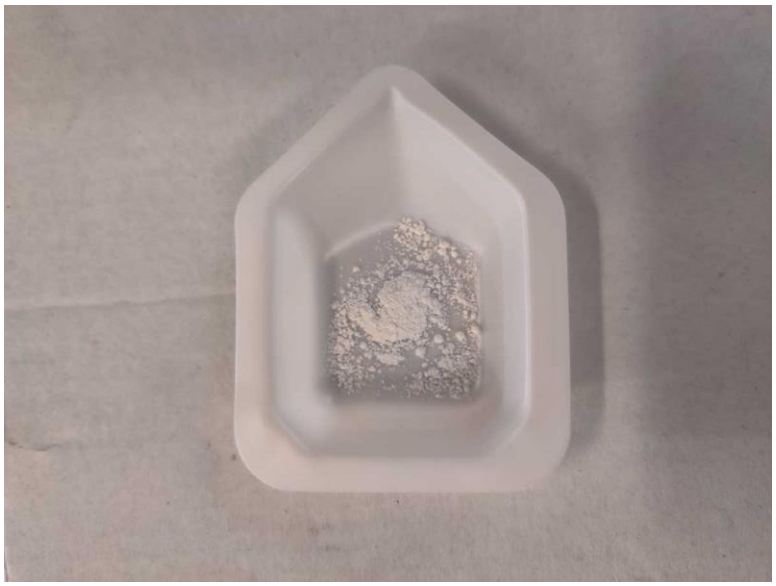

Figure 16. ZnO nanoparticles used in our experiments.

2.1.3 N,N-dimethylformamide (DMF). There are different kinds of solvents such as acetone, N-Methyl-2-Pyrrolidone (NMP), Hexamethylphosphoramide (HMPA), tetrahydrofuran (THF), methyl ethyl ketone (MEK), and DMF that can be used to dissolve PVDF [81, 82]. Because of each solvent's properties, using these solvents shows different effects on the crystallization of PVDF chains [83].

In 2008, Ma et al. [83] used three of these solvents, DMF, MEK, and THF, to show their effect on PVDF and its crystal β-phase content. They concluded that using DMF as a solvent gave the highest β-phase crystallization in PVDF. The same author also illustrated that the MEK-based process favored the β-phase crystallization in PVDF more than the THF process. Moreover, PVDF was fully dissolved in DMF while only partially dissolved in MEK and THF.

One of the important parameters of a PVDF solvent is for it to have a slow evaporation rate, which is desired for obtaining the β-phase [81]. DMF is a solvent that has a high boiling point and evaporates relatively slowly [84]. Also among all these solvents, DMF is the most common and efficient solvent for PVDF [85]. In order to evaluate material options for us to find the right solvent, we used MEK, DMF, and acetone in our experiments. Each of the solvents was mixed using the magnetic stirring method with the same amount of PVDF powder in separate beakers at 70°C. The solution with DMF provided the best result in dissolving the PVDF (Figure 17a). The PVDF powder was entirely dissolved and the solution was uniform. Figure 17b shows the result from using acetone to dissolve the PVDF powder. The majority of PVDF was undissolved. The undissolved PVDF powder can also be seen in Figure 17c when MEK was used as the solvent. Therefore, DMF was chosen as the primary solvent in dissolving

the PVDF powder for the following experiments. The DMF (99% ACS) product was obtained from VWR.

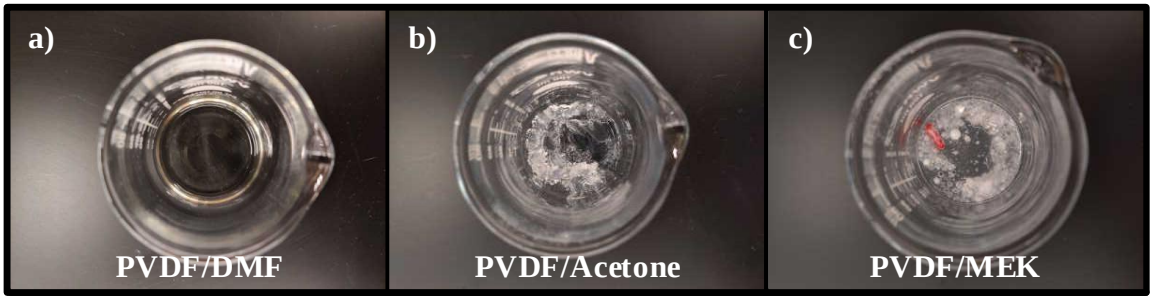

Figure 17. Comparison of solvents in dissolving PVDF. For each experiment, 1 g PVDF is mixed with 5 mL solvent. a) DMF. b) Acetone. c) MEK for 50 minutes at 70°C under magnetic stirring.

2.1.4 Methyl ethyl ketone (2-butanone / MEK). MEK was used for two different purposes. As previously mentioned, DMF was used to dissolve PVDF powder. However, using DMF alone resulted in relatively rigid and flimsy PVDF thin-film samples. Therefore, using a second solvent became a necessary option to have softer, more flexible thin-film samples. In 2009, Zhao et al. [90] illustrated that using mixed solvents, ethanol and DMF, at different ratios had different effects on the crystal phases in PVDF as well as its morphology. Thus, we started to experiment with mixing different ratios of multiple solvents. At the end, it appeared that using additional MEK in the mixed solvents was able to produce less rigid thin-film samples than using only DMF as the solvent. Moreover, adding MEK could reduce the dissolving time of PVDF. Previous studies have shown that the best temperature to dissolve PVDF is between 60-70°C in order to have a uniform solution without the loss of β-phase content [81, 83, 86].

Therefore, three temperatures at 60°C, 65°C and 70°C were experimented to find the optimal condition for material processing. Table 4 shows that 70°C was the optimal temperature for dissolving the PVDF. It also illustrates that higher temperature affects the dissolving time as well.

Table 4

The effect of using different solvents and dissolving temperatures on PVDF solution

Picture	Parameters		Results
	**PVDF**	1.00 g	After 230 min magneting stirring, PVDF was entirely dissolved. This solution had a brittle morphological structure after leaving it in open-air for 2 days.
	Solvent-1 (DMF)	5.00 mL	
	Solvent-2 (MEK)	-	
	Temperature	60 °C	
	Mag. Stirring Time	230 min.	
	**PVDF**	1.00 g	After 180 min magneting stirring, PVDF was entirely dissolved. The stirring time goes down by 50 min. after adding MEK. Also, the morphological structure wasn't realy brittle compare to the solution without MEK.
	Solvent-1 (DMF)	4.00 mL	
	Solvent-2 (MEK)	1.00 mL	
	Temperature	60 °C	
	Mag. Stirring Time	180 min.	
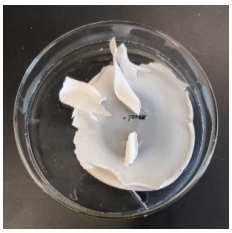	**PVDF**	1.00 g	After 150 min magneting stirring, PVDF was entirely dissolved. At 60°C it took 230 min. to dissolve. Thus, increasing temperature 5°C helped to decreas the dissolving time 80 min. The final solution had a brittle morphological structure after leaving it in open-air for 2 days.
	Solvent-1 (DMF)	5.00 mL	
	Solvent-2 (MEK)	-	
	Temperature	65 °C	
	Mag. Stirring Time	150 min.	
	**PVDF**	1.00 g	After 100 min. magneting stirring, PVDF was entirely dissolved. Thus, adding MEK decreased the dissolving time 50 min. Moreover, adding MEK perceptibly took the brittle morphological structure away.
	Solvent-1 (DMF)	4.00 mL	
	Solvent-2 (MEK)	1.00 mL	
	Temperature	65 °C	
	Mag. Stirring Time	100 min.	
	**PVDF**	1.00 g	After 80 min magneting stirring, PVDF was entirely dissolved. The stirring time decreased from 100 min. to 80 min. The morphological structure was brittle after leaving it in open-air for 2 days.
	Solvent-1 (DMF)	5.00 mL	
	Solvent-2 (MEK)	-	
	Temperature	70 °C	
	Mag. Stirring Time	80 min.	
	**PVDF**	1.00 g	After 50 min magneting stirring, PVDF was entirely dissolved. The stirring time decreased from 80 min. to 50 min. by increasing the temperature from 65°C to 70°C. The morphological structure wasn't brittle after leaving it in open-air for 2 days.
	Solvent-1 (DMF)	4.00 mL	
	Solvent-2 (MEK)	1.00 mL	
	Temperature	70 °C	
	Mag. Stirring Time	50 min.	

The second reason to use MEK in the process was to disperse ZnO NPs. Previous reports showed that acetone, MEK, ethanol, dimethyl sulfoxide (DMSO), and n-Propylamine (PA) are good solvents to disperse ZnO [43, 87-90]. In this study, acetone, ethanol, and MEK were investigated as dispersing solvents for ZnO NPs. In these experiments, 7% (0.07 g) of ZnO NPs was mixed with each one of these solvents separately and sonicated for 1h, 2h, and 3h. Figure 18a and Figure 18b show the dispersion results from using acetone and ethanol, respectively. After three hours of sonication, the majority of ZnO NPs were not dispersed in either solvent. By comparison, it can be seen in Figure 18c that the MEK provided the best result after three hours of sonication. However, using only MEK was not sufficient to disperse the ZnO NPs entirely. Therefore, mixing the dissolved PVDF and ZnO/MEK solution became a viable option. It can be seen in Figure 18d that mixing MEK/ZnO solution with the PVDF solution and then sonicating for three hours provided the best result.

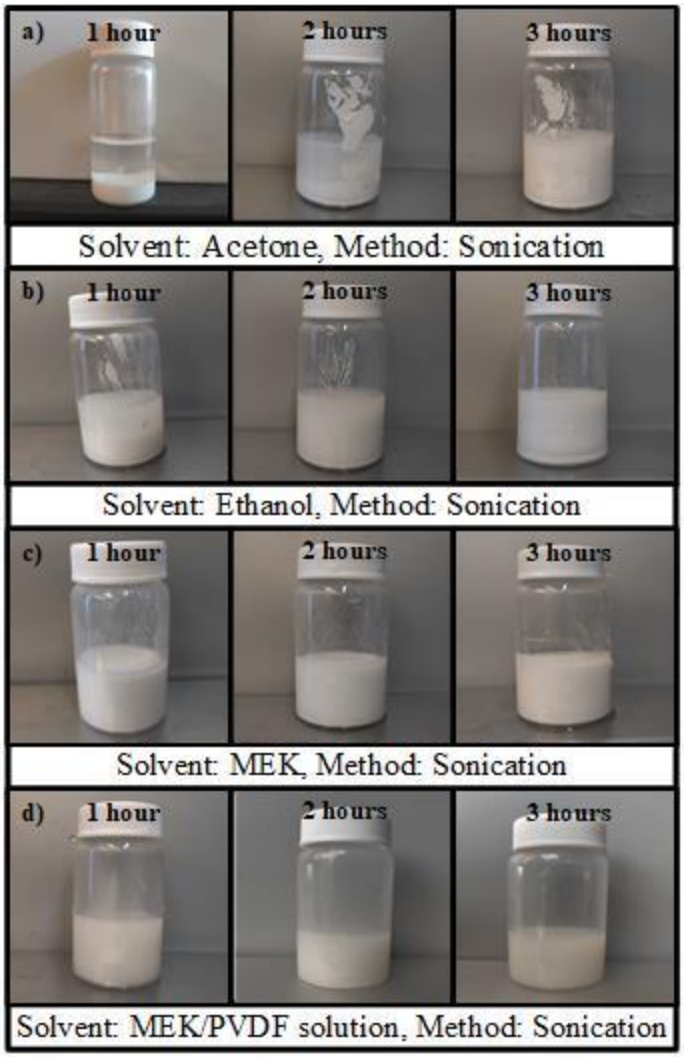

Figure 18. Comparison of solvents in disperse ZnO NPs. For each experiment, 7% (0.07 g) ZnO NPs are mixed with 5 mL solvents in a 20 mL vial glass and then sonicated for 1h, 2h, and 3h. a) Acetone. b) Ethanol. c) MEK. d) MEK/PVDF solution.

2.2 Sample Fabrication

2.2.1 Preparation of PVDF/ZnO solution. Four different composite samples were prepared using different ZnO NPs contents in PVDF. The recipes are summarized in Table 5.

Table 5

The PVDF/ZnO NPs recipes

PVDF (g)	ZnO NPs (mg)	DMF (mL)	MEK (mL)
1	0 (0%) 30 (3%) 50 (5%) 70 (7%)	4	6

The process for dissolving PVDF power is illustrated in Figure 19. To prepare the PVDF solution, 4mL DMF and 1mL MEK are mixed in a 100 mL glass beaker to dissolve 1g PVDF powder. The beaker is placed on a hot plate which is set at 70°C. The temperature of the hot plate is important because it affects the β-phase crystallization in PVDF. Once the mixed solvent's temperature reaches 70°C, PVDF powder is added into the beaker. PVDF powder is evenly dispersed in three parts as it prevents the PVDF powder to agglomerate together. This ensures uniform dispersion of PVDF in the solution. The beaker is covered with aluminum foil to prevent solvent evaporation. The solution is magnetically stirred until the PVDF is entirely dissolved (~ 50 minutes) (Figure 19 and Figure 20)

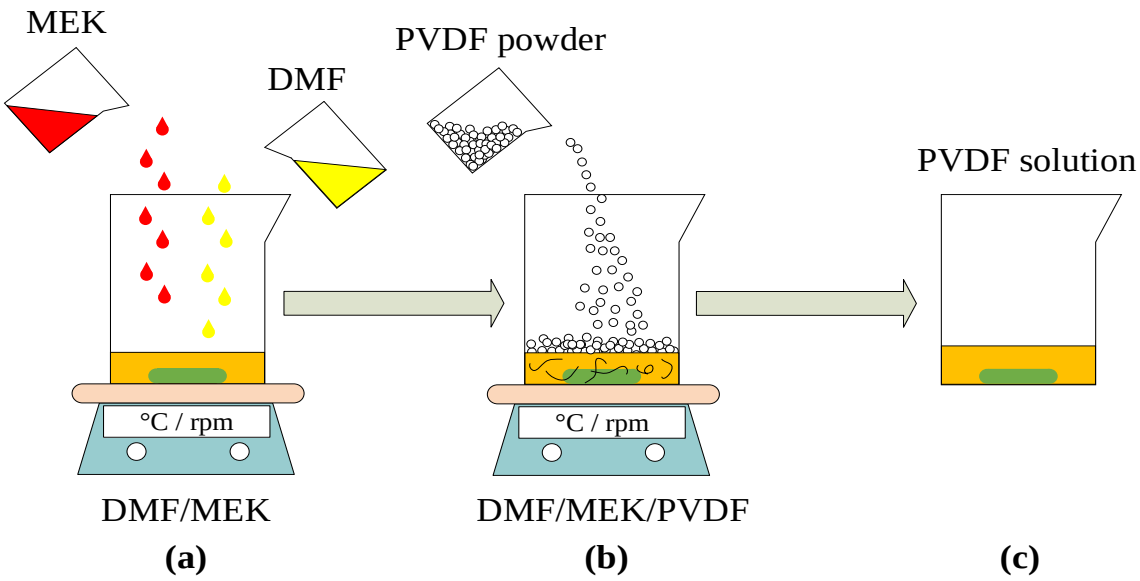

Figure 19. Dissolving method for PVDF. a) MEK and DMF are poured into a beaker. The beaker is placed on a hot plate which is set at 70°C. b) Once the solvent's temperature reaches 70°C, PVDF is poured into the beaker and stirred at 300 rpm for 50 min. c) Uniform PVDF solution.

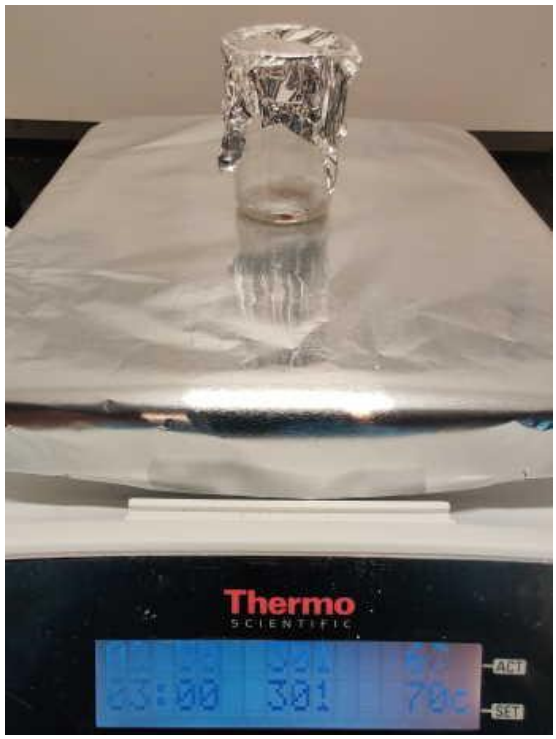

Figure 20. PVDF powder is being dissolved in DMF and MEK.

After PVDF is completely dissolved, the next step is to disperse the ZnO NPs. For this process, 5 mL MEK is poured inside a separate 20 mL glass vial and placed on the hot plate until its temperature reaches 70°C. ZnO NPs are poured in the glass vial and mixed with the PVDF solution. This PVDF/ZnO solution is placed into a sonication machine to help disperse the ZnO NPs. Sonication takes between 4-6 hours depending on the concentration of ZnO NPs (3%, 5%, and 7%). When the ZnO NPs are completely dispersed, the PVDF/ZnO solution is poured into an 80mL glass beaker with a stir bar. Figure 21 shows the schematic of the entire process from preparing the ZnO solution to de-bubbling the final solution before spin coating. A similar process is applied to the preparation of pure PVDF samples, except the steps for adding ZnO NPs and sonication.

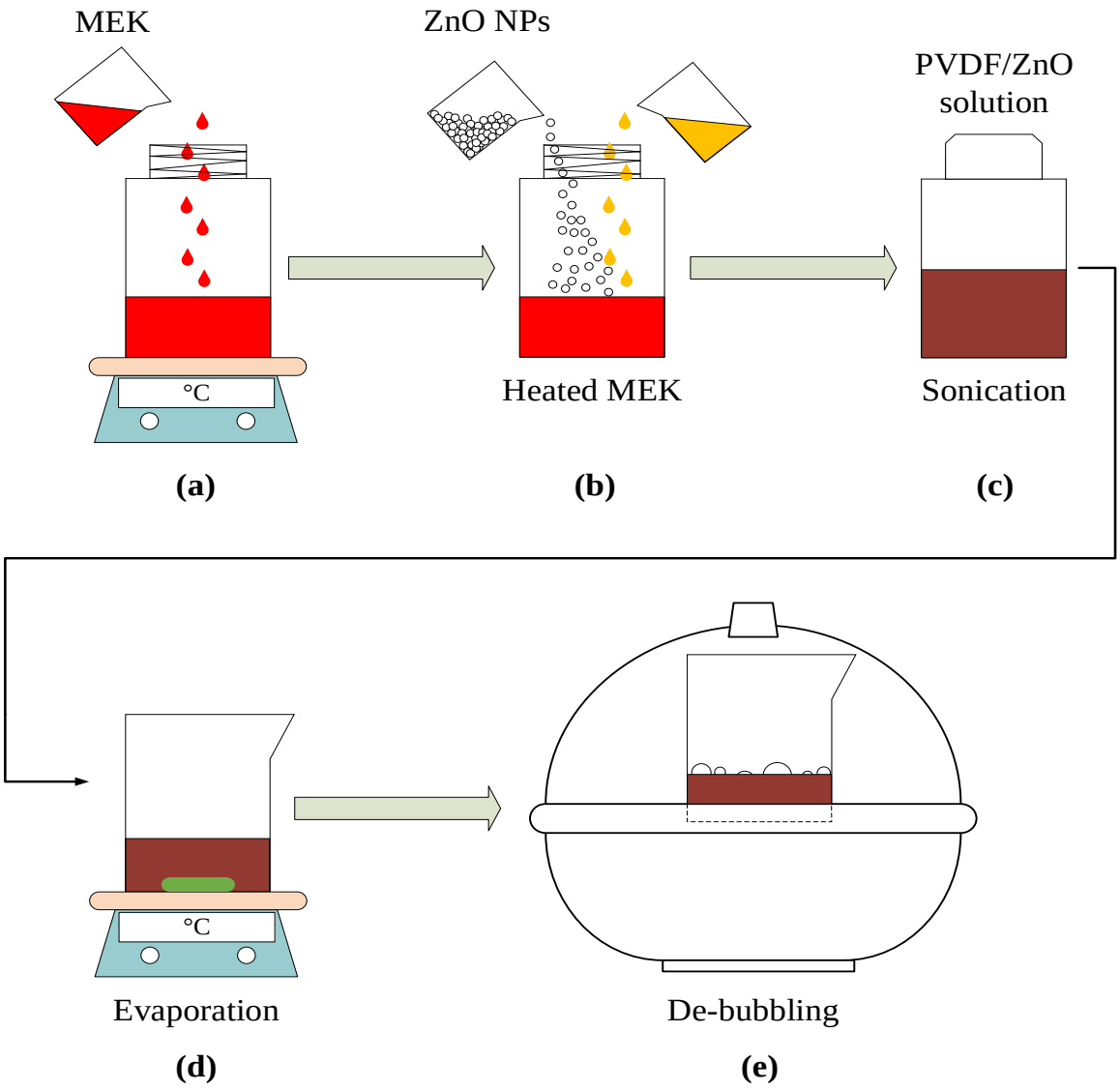

Figure 21. Preparation of PVDF/ZnO solution. a) MEK is poured in a 20 mL glass vial and heated up. b) ZnO NPs and PVDF solution are mixed in the glass vial. c) The glass vial is placed in sonication machine. d) PVDF/ZnO solution is poured in a beaker and placed on a hot plate for evaporation process. e) A vacuum desiccator is used for the de-bubbling process.

The PVDF/ZnO NPs solution is placed onto a hot plate to evaporate the solvents at 90°C/300rpm. (Figure 22a). The evaporation process takes approximately 15 minutes, as longer evaporation resulted in a thick solution and shorter evaporation resulted in a

watery solution. During the evaporation process, bubbles are present in the solution. Having bubbles inside the solution affects the film quality as the film is not uniform. Therefore, a vacuum desiccator is used for the de-bubbling process (Figure 22b). After removing all the bubbles, the PVDF/ZnO NPs solution is ready for the spin coating process.

Figure 22. a) Evaporation of solvents from the PVDF/ZnO solution. b) The PVDF/ZnO solution in a de-bubbler after the evaporation process.

2.2.2 Spin coating and annealing. Thin-film energy harvesters are fabricated using the spin coating fabrication method. A schematic of the spin coating and the following annealing process can be seen in Figure 23.

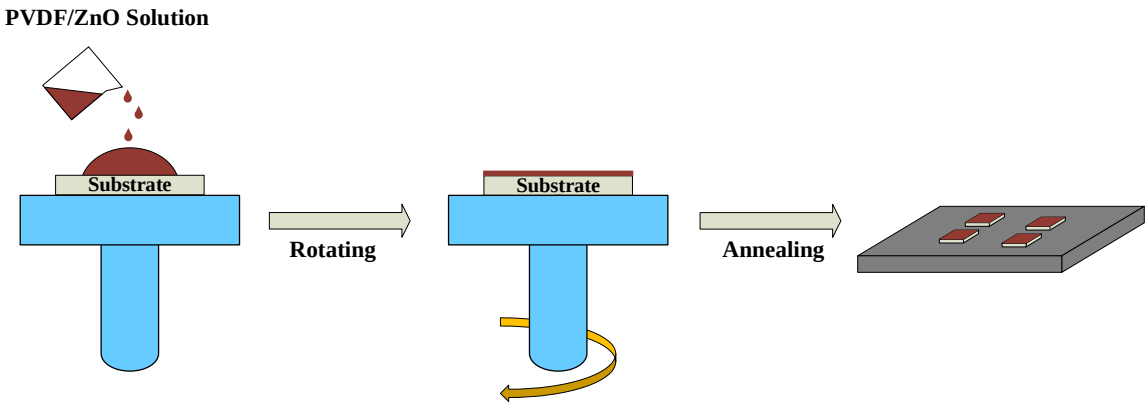

Figure 23. Spin coating and annealing process to create thin-film samples.

To obtain thin-film energy harvesters, PVDF/ZnO solution is spin coated onto 2.5 cm × 2.5 cm glass slides. The spin speed is set as 500 rpm for 30 seconds, then 1000 rpm for 30 seconds, and finished at the maximum speed of 1500 rpm for 30 seconds (Figure 24a). After the spin coating process, glass slides are moved onto a hot plate, which is set at 90°C, to anneal for 3 hours (Figure 24b). When the annealing is done, thin-film samples can be peeled off from the glass slide substrates.

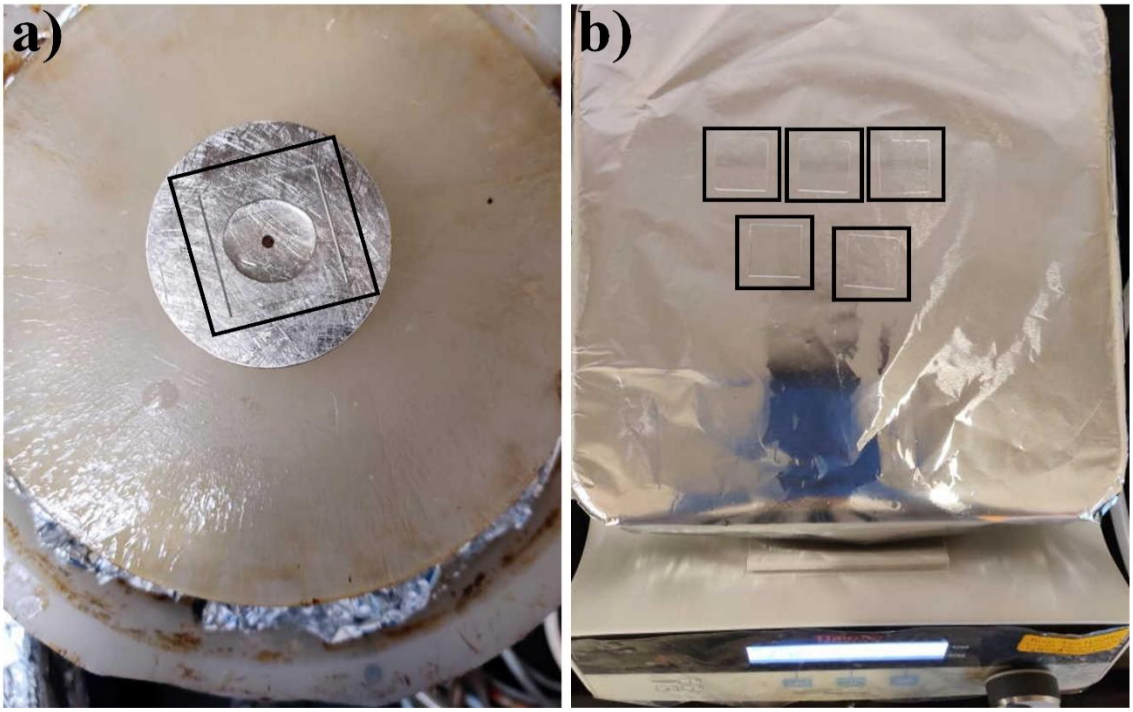

Figure 24. a) Spin coating of PVDF solvent on a glass substrate. b) Annealing process of the spin coated films on a hot plate.

Figure 25 shows the obtained thin-film energy harvester samples. The thicknesses of thin-films are around 15-20 µm. Although these samples differ in appearances due to the various concentrations of ZnO NPs, each sample is uniform in thickness and color with no visible defects. These thin-film samples are ready for further testing as individual devices.

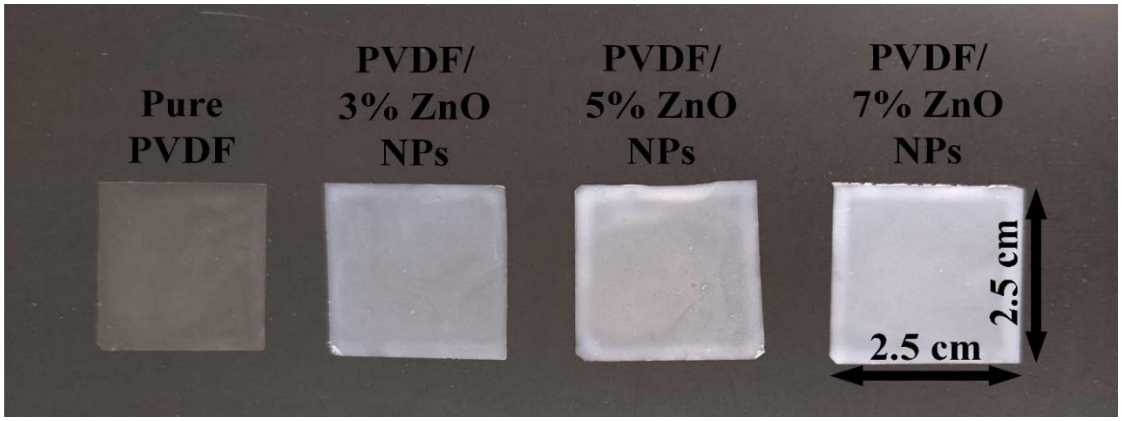

Figure 25. PVDF based thin-film energy harvesters with different ZnO NP concentrations.

Chapter 3

Mechanical Characterization of Thin-Film Energy Harvesters

As mentioned previously, integrating ZnO NPs inside the PVDF affects the piezoelectric properties of resulting energy harvesters. At the same time, changing the ZnO NPs concentrations also has effects on thin-film energy harvesters' mechanical properties, such as their Young's modulus [91]. For this set of experiments, tensile testing was used to obtain the strain-stress curves of PVDF and PVDF/ZnO composite films. Other critical mechanical parameters such as Young's modulus and ultimate strength are derived from the stress-strain curves.

3.1 Tensile Testing

The tensile testing of the films was performed using a combination of a tabletop SHIMPO MTS system, an FGV-50XY force gauge, two clamps, a computer, and a software package to transfer the data. Figure 26a shows the system setup. Since the samples' thickness was relatively low, around 15-20 μm, it was difficult to grip them using existing clamps. Therefore, additional rubber sheets were placed on the clamps to enhance the gripping power (Figure 26b).

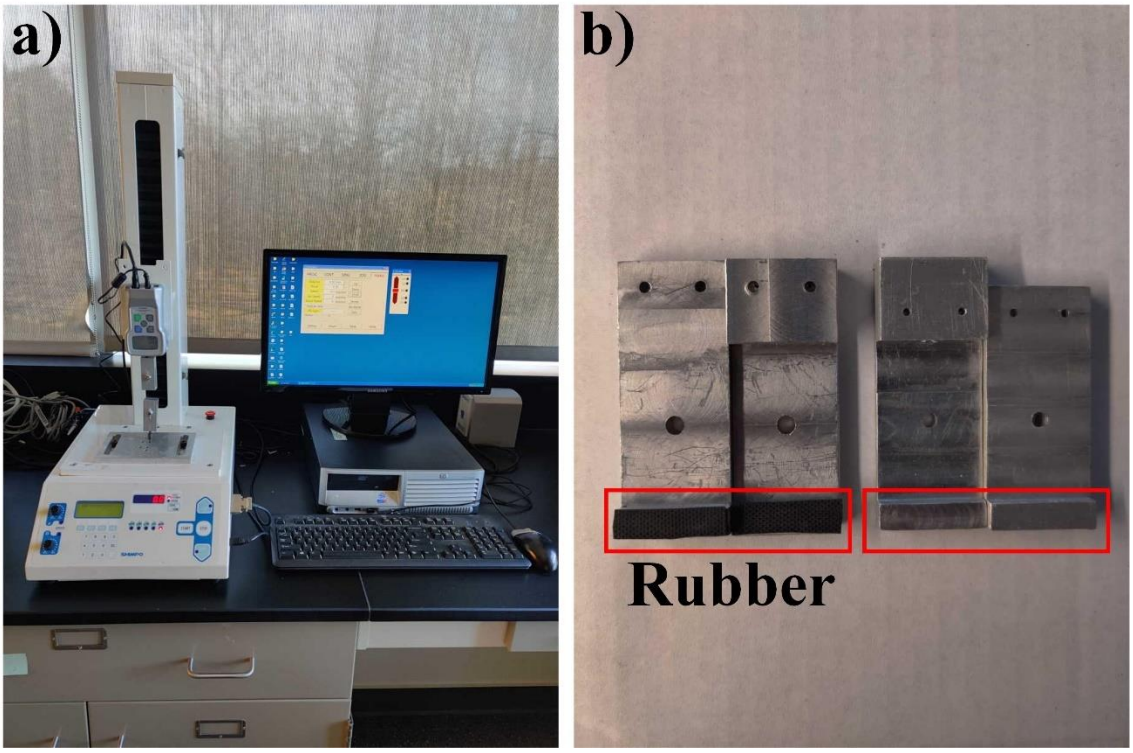

Figure 26. a) SHIMPO tensile testing setup. b) Rubber sheets are used to provide strong gripping on thin-film samples.

Figure 27 shows a sample placed between the two clamps: one (bottom clamp) is a stationary ground clamp and the other one (top clamp) is connected to the force gauge. Once the sample was properly mounted and the control program parameters were set, the thin-film sample was slowly pulled apart until it broke off. The force gauge was used to record the force data and the SHIMPO MTS was used to record the displacement data using the computer software. Using the initial geometry of the thin-film sample (1.5 cm × 2.5 cm), the recorded force and displacement data were converted into stress and strain values, respectively. For statistical analysis, the data were collected from five different samples for each ZnO NP concentration. The stress-strain diagrams for different ZnO

NPs concentrations were acquired by plotting these stress and strain values against each other.

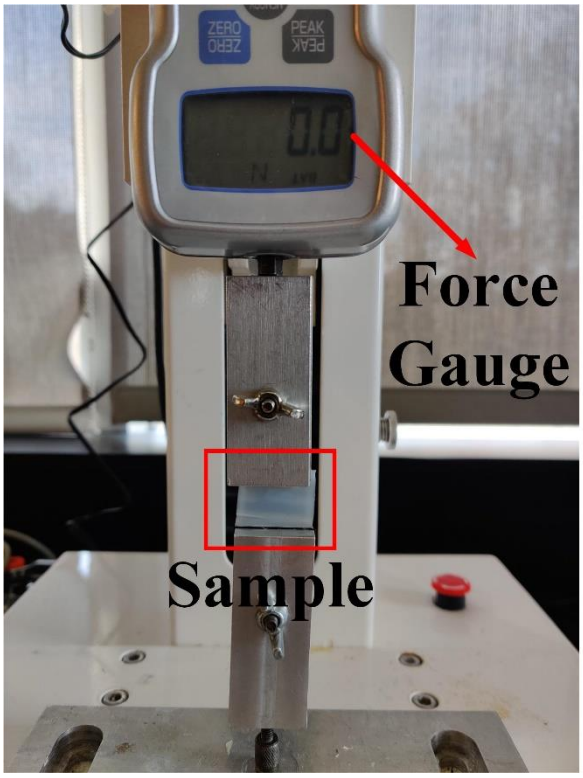

Figure 27. A mounted sample on the tensile tester.

3.2 Results and Discussion

Tensile testing is used to investigate how different concentrations of ZnO NPs affect the mechanical properties of thin-film energy harvesters. After running several sets of experiments on various samples, Young's modulus for each sample was calculated using the stress-strain data from these measurements. Figure 28 shows the stress-strain diagrams of four thin-film samples with 0%, 3%, 5%, and 7% ZnO NPs embedded in the host PVDF. The results show that integrating ZnO NPs has observable effects on thin-films' strain-stress responses. It is obvious that the PVDF thin-film sample with 3% ZnO NPs concentration exhibited the highest ultimate stress at 62.3 MPa and provided the best

flexibility. The PVDF sample with 5% ZnO NPs exhibited the lowest ultimate stress at 28.8 MPa. Interestingly, adding 7% ZnO NPs resulted in a slightly increased ultimate stress at 30.07 MPa. The pure PVDF sample's ultimate stress was measured at 44.8 MPa. It can be seen that the samples with 0% and 3% ZnO NPs can withstand larger structural deformation with more elastic-material-like behaviors, while the samples with 5% and 7% ZnO NPs show sudden material fracture right after the ultimate stress point, exhibiting brittle-material-like behaviors.

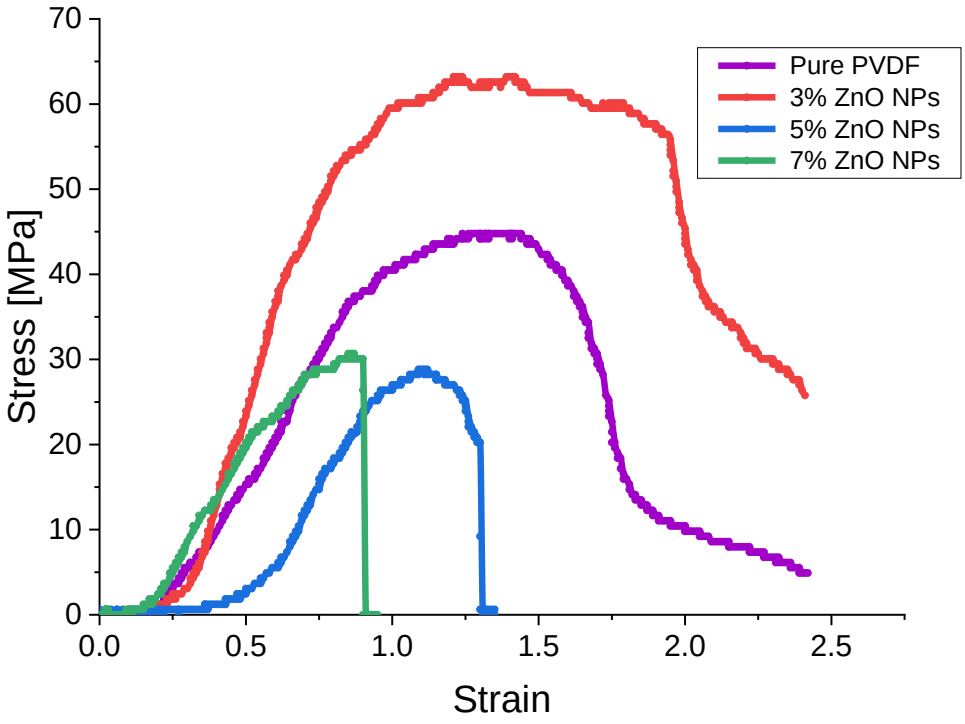

Figure 28. Stress-strain curves for the PVDF thin-film samples with different ZnO NP concentrations.

Figure 29 shows the mean and the standard deviation values of Young's modulus for each ZnO NPs concentration. The PVDF samples with 3% ZnO NPs exhibited the

highest average Young's modulus of 1334.92 MPa, followed by the PVDF samples with 5% ZnO NPs and the pure PVDF samples. The PVDF samples with 7% ZnO NPs had the lowest Young's modulus of 944.21 MPa. Moreover, the standard deviation error bars showed significant overlapping between pure PVDF, 3% PVDF/ZnO, and 5% PVDF/ZnO samples. This suggests that there are no statistically significant differences among these samples. However, the PVDF samples with 7% ZnO NPs showed the smallest standard deviation value and it does not overlap with any other standard deviation error bars. This suggests that the 7% ZnO NPs sample has the most consistent stiffness in our measurements. Because these samples rely on piezoelectricity where electrical signals are generated under mechanical deformations, it is therefore important to obtain the mechanical behaviors of these samples with consistent measurement results.

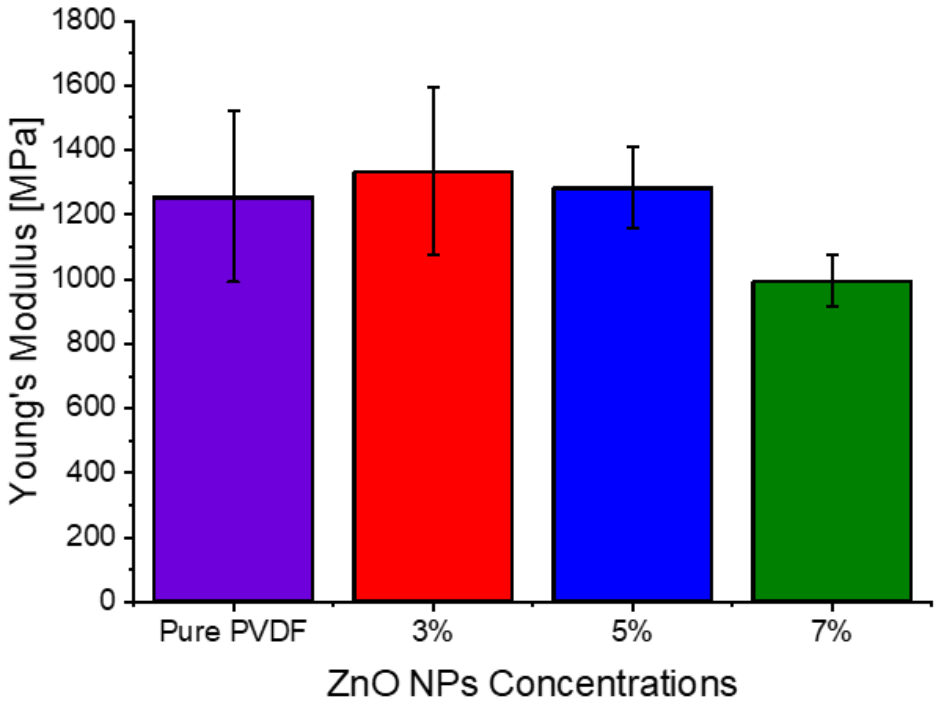

	Pure PVDF (MPa)	3% ZnO NPs (MPa)	5% ZnO NPs (MPa)	7% ZnO NPs (MPa)
Mean	1257.22	1334.92	1284.58	994.21
Std. Deviation	265.64	259.45	127.41	79.29

Figure 29. The Young's modulus, including the mean values and the error bars, for pure PVDF and PDVD/ZnO composite samples.

Overall, these results show that the PVDF samples with 3% ZnO NPs represent the strongest and the most elastic material, whereas the samples with 7% ZnO NPs are the most brittle material. The stiffness of the samples remains relatively consistent when the concentrations of ZnO NPs are low, up to 5%. By comparison, the 7% PVDF/ZnO NPs samples show a reduced stiffness. Nonetheless, all these samples demonstrate sufficient flexibility and mechanical strength for piezoelectric energy harvesting applications.

Chapter 4

Electrical Characterization of Thin-Film Energy Harvesters

4.1 Polarization

One way to improve the piezoelectric properties of PVDF thin-film samples is to polarize them through electrode poling. The method of polarizing the sample, or polarization, can be defined as a process to align the orientation of dipoles, or randomly oriented polarization directions (Figure 30), in piezoelectric polymer thin-film samples by applying a high external electric field [41, 72, 92]. To achieve successful polarization, the poling time, the applied external electric field strength, and the poling temperature are important factors [93]. The uniform polarization is usually achieved by poling thin-film samples for a long period of time at 90°C and above. The poling time depends on the thicknesses of the samples. The typical electric field strength for efficient poling of piezo-polymers is between 50-120 MV/m (or V/μm) [92, 94]. The polarization of the PVDF sample can be maintained below the Curie temperature (T_c = ~110°C for PVDF). In other words, the β-phases of PVDF turn into α-phases when the applied temperature is higher than T_c [95].

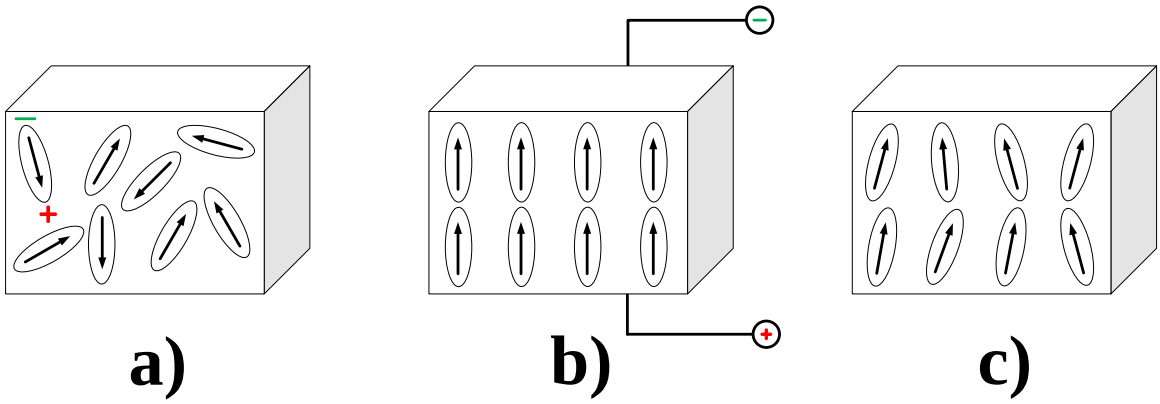

Figure 30. The electrode poling process to align dipoles in a material. a) Randomly oriented polar axis of domains prior to polarization. b) Reorientation of dipoles when a high electric field is applied. c) Remainder polarization after the poling treatment.

There are different types of poling techniques with corona poling and electrode poling being the two most common methods for polymer energy harvesters [92, 96]. In particular, electrode poling is considered as the easiest method to perform. A schematic of the electrode poling setup can be seen in Figure 31.

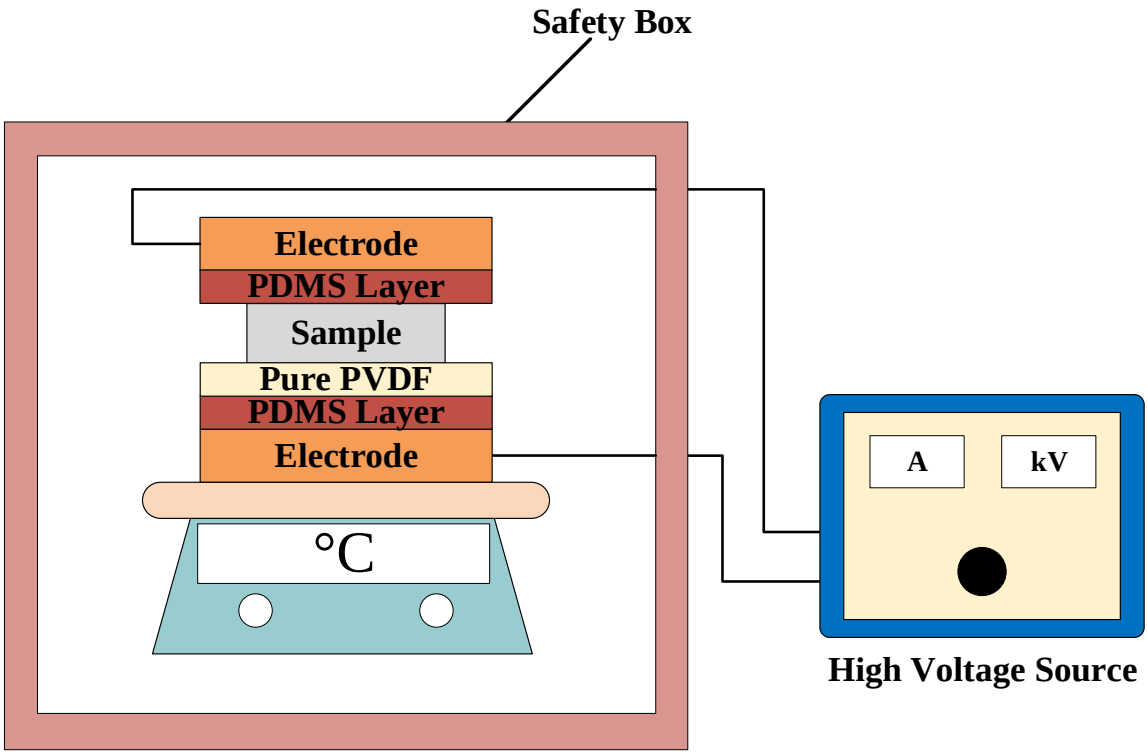

Figure 31. Schematic of the electrode poling setup.

This method requires a high voltage source, two parallel plate electrodes, a hot plate, and a safety box in a vacuumed environment. The vacuumed environment is typically needed to avoid the arcing between electrodes, which can cause material or system breakdown. However, to simplify the system, we included insulation layers around the electrodes, so our poling setup did not require a vacuumed environment. A large piece of pure PVDF thin-film sample was used to cover the entire surface area of the copper plates. This thin-film sample was used to avoid the contact between the electrodes. Moreover, we used polydimethylsiloxane PDMS as an insulator for coating the copper plates [97]. The electrode poling setup used for our experiments is shown in Figure 32.

Figure 32. The poling setup used for the experiments.

The poling process starts with removing the safety box, placing the sample between the copper plates, and placing the copper plates onto a hot plate. The hot plate's temperature is set at 160°C to be able to have the temperature between copper plates at 140°C. A thermocouple is used to monitor the temperature between the copper plates. After connecting the hot and ground wires from the voltage source to copper plates, the hot plate is covered with the safety box and then the power source is turned on. The voltage value is carefully increased until the calculated value is reached. In order to avoid arcing and ensure there is no system breakdown, the poling process is closely monitored. Whenever arcing appears, the applied voltage value should be decreased. Our poling parameters are summarized in Table 6.

Table 6

Electrode poling parameters

Poling Temperature	Applied Electric Field	Poling Time
140°C	100 V/μm	40 minutes

The equation to calculate the strength of the applied electric field is below.

$$E = V \div d \quad (2)$$

***E*:** The electric field strength (V/μm)

***V*:** The voltage supplied (V)

***d*:** The distance (μm) between the two plates

4.2 Electrical Testing Setup

The electrical properties of the thin-film energy harvester samples are obtained using an electro-mechanical testing system that includes an amplifier, a waveform generator, a shaker (vibration generator), two data acquisition units (DAQ; one for voltage measurements and the other for current measurements), a computer, and a breadboard circuit. The system setup can be seen in Figure 33.

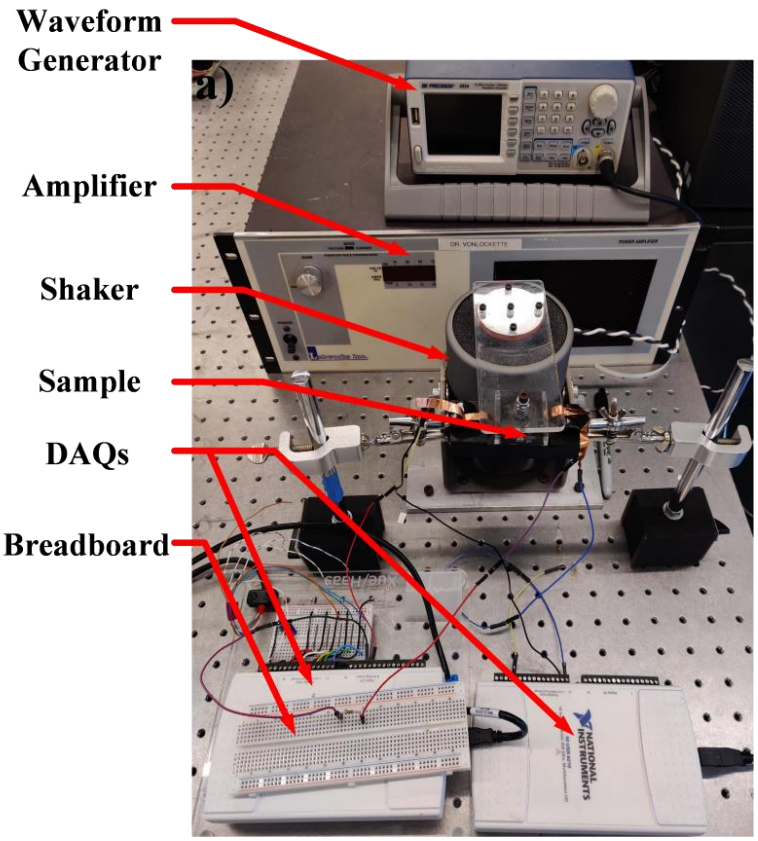

Figure 33. Electrical testing setup.

Figure 34a shows the flow chart of the setup. The waveform generator and amplifier are used to activate the shaker. The waveform generator generates a sinusoidal signal with its frequency and amplitude set at proper levels. The signal amplifier amplifies the input signal to enable the shaker to work for the testing purpose. When the shaker starts moving up and down, the sample deformation starts (Figure 34b-c). Figure 34d shows where the samples are placed to undergo mechanical deformation. Because of this mechanical deformation, the sample starts producing electrical energy in the form of both voltage and current. Two electrodes (copper tape), which are connected to the DAQs through the breadboard, collect the electrical signals and transfer the data to the DAQs,

which further send the results to the computer. The voltage and current output signals are recorded and displayed on the computer monitor using the LabVIEW code.

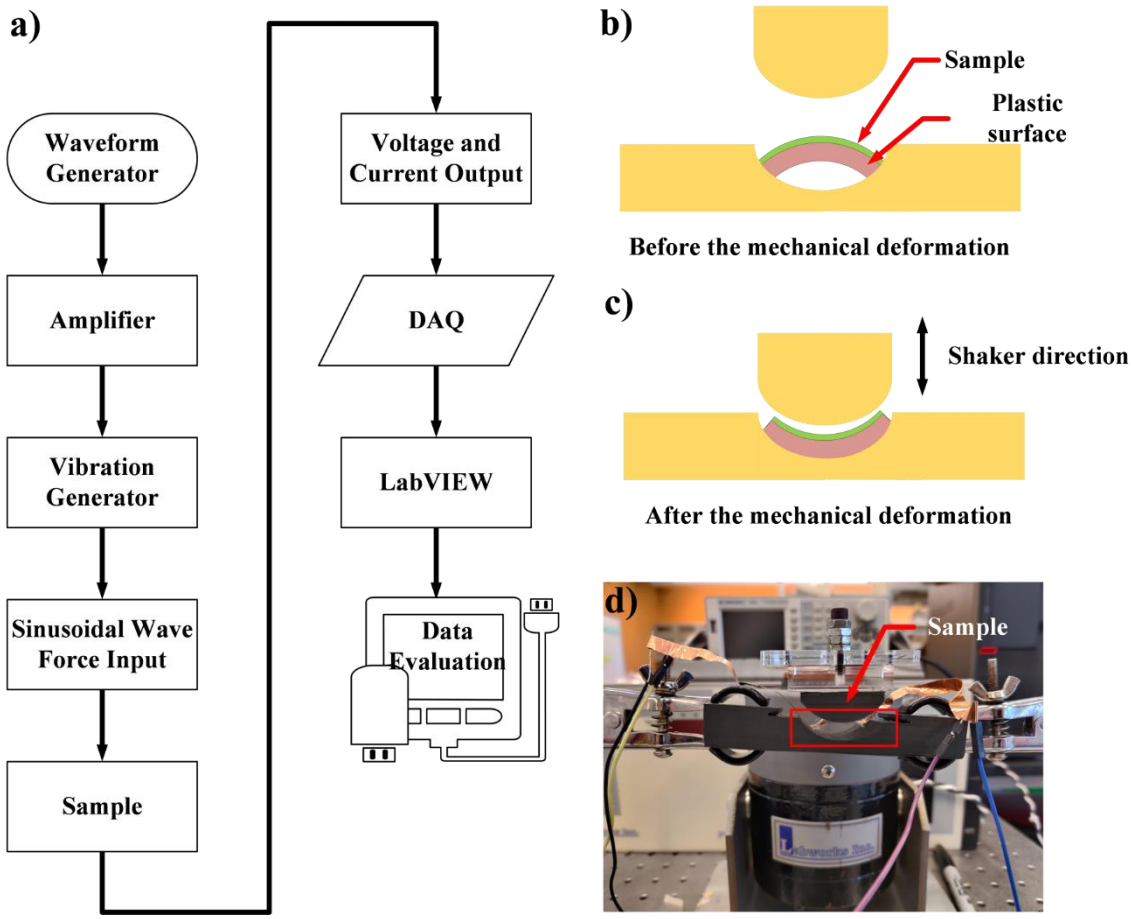

Figure 34. a) Flow chart of electrical testing setup. b) Initial state of the sample without mechanical force. c) The deformed sample under applied force. d) Closer view of sample placement.

4.3 Electrical Testing Results

For this set of experiments, the goal was to measure the voltage and current outputs from the same sample simultaneously. The circuit for electrical measurement can

be seen in Figure 35. The voltage and current measurements were taken simultaneously from the sample by two DAQs.

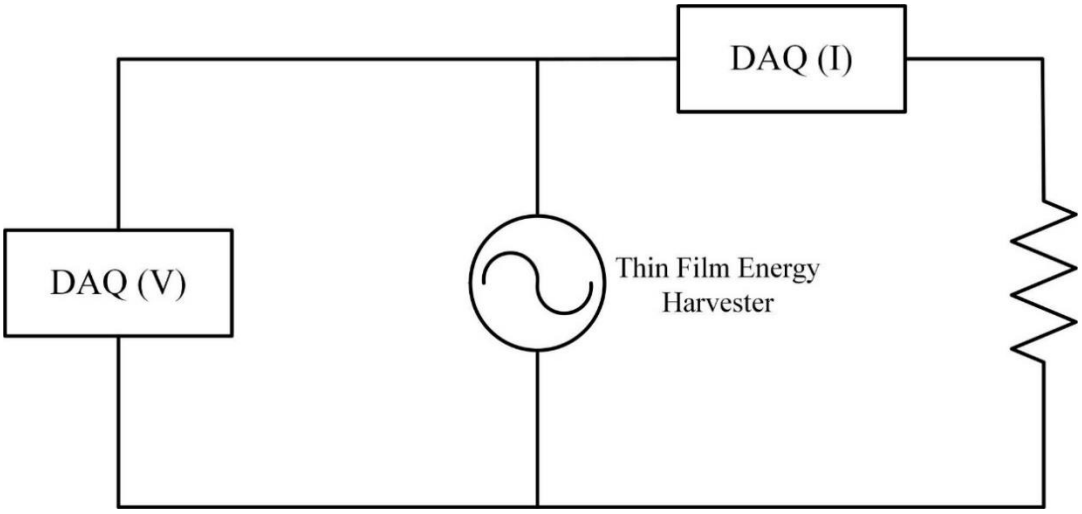

Figure 35. Circuit for taking voltage and current measurements simultaneously.

To find the proper resistor value to ensure accurate data collection, different resistors with the resistance of 1 kΩ, 2 kΩ, 5 kΩ, 10 kΩ, 100 kΩ, and 1 MΩ were tested on the circuit. In the end, the 1 MΩ resistor provided the most consistent reading for both the voltage and current measurements. Therefore, the 1 MΩ resistor was used in further experiments.

The short-circuit current (I_{sc}) and open-circuit voltage (V_{oc}) are collected at 7 Hz frequency. The impact of different concentrations of ZnO NPs on the electrical properties of unpoled thin-film energy harvesters can be seen in Figure 36. The pure PVDF sample showed V_{oc} ~1 V and I_{sc} ~2.5 mA. Integrating 3% ZnO NPs in our solution increased the V_{oc} from ~1 V to 1.5 V. Increasing the ZnO NPs content up to 5% did not show a

significant effect on the voltage output from the sample with 3% ZnO NPs. However, adding 7% ZnO NPs in PVDF enhanced the V_{oc} to 3.5 V and I_{sc} to ~9 mA, both of which showed considerable amounts of output enhancement.

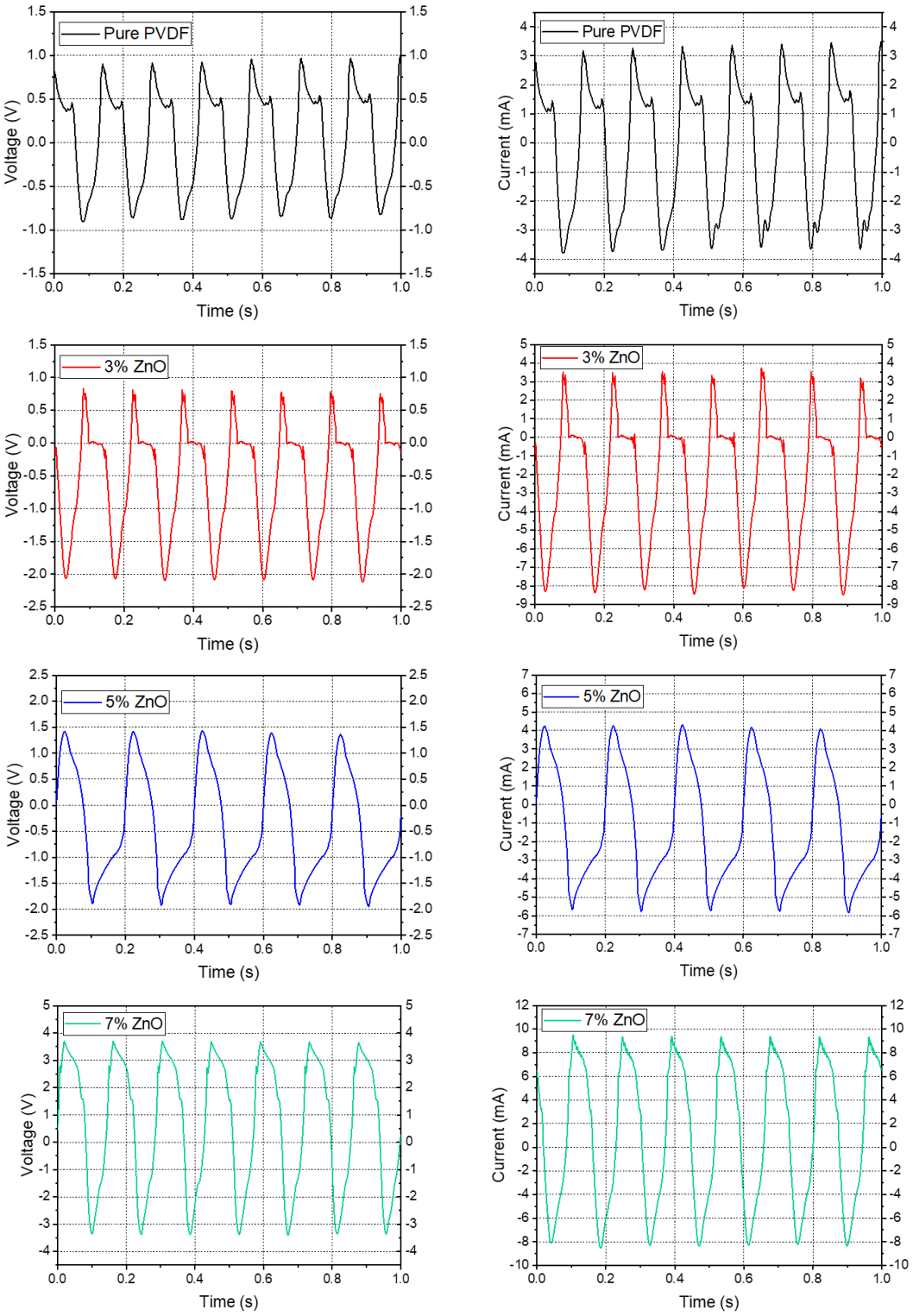

Figure 36. Open-circuit voltage and short-circuit current of unpoled PVDF thin-film energy harvester with different ZnO NPs contents.

The same electrical measurements were done after electrode poling as well. The results can be seen in Figure 37. The results show that the poled thin-film samples exhibit higher electric output. After the electrode poling process, the V_{oc} for the poled pure PVDF increased up to 2.65 V, which was almost three times higher than that for the unpoled thin-film samples. The PVDF thin-film sample with 3% ZnO NPs content's voltage output reached up to 2.75 V from 1.5 V after polarization. The voltage output of the thin-film sample with 5% ZnO NPs enhanced from 1.6 V to 4.5 V after dipole alignment. The poled PVDF thin-film sample with 7% ZnO NPs content exhibited the highest V_{oc} and I_{sc} at 5.6 V and ~20 mA, respectively.

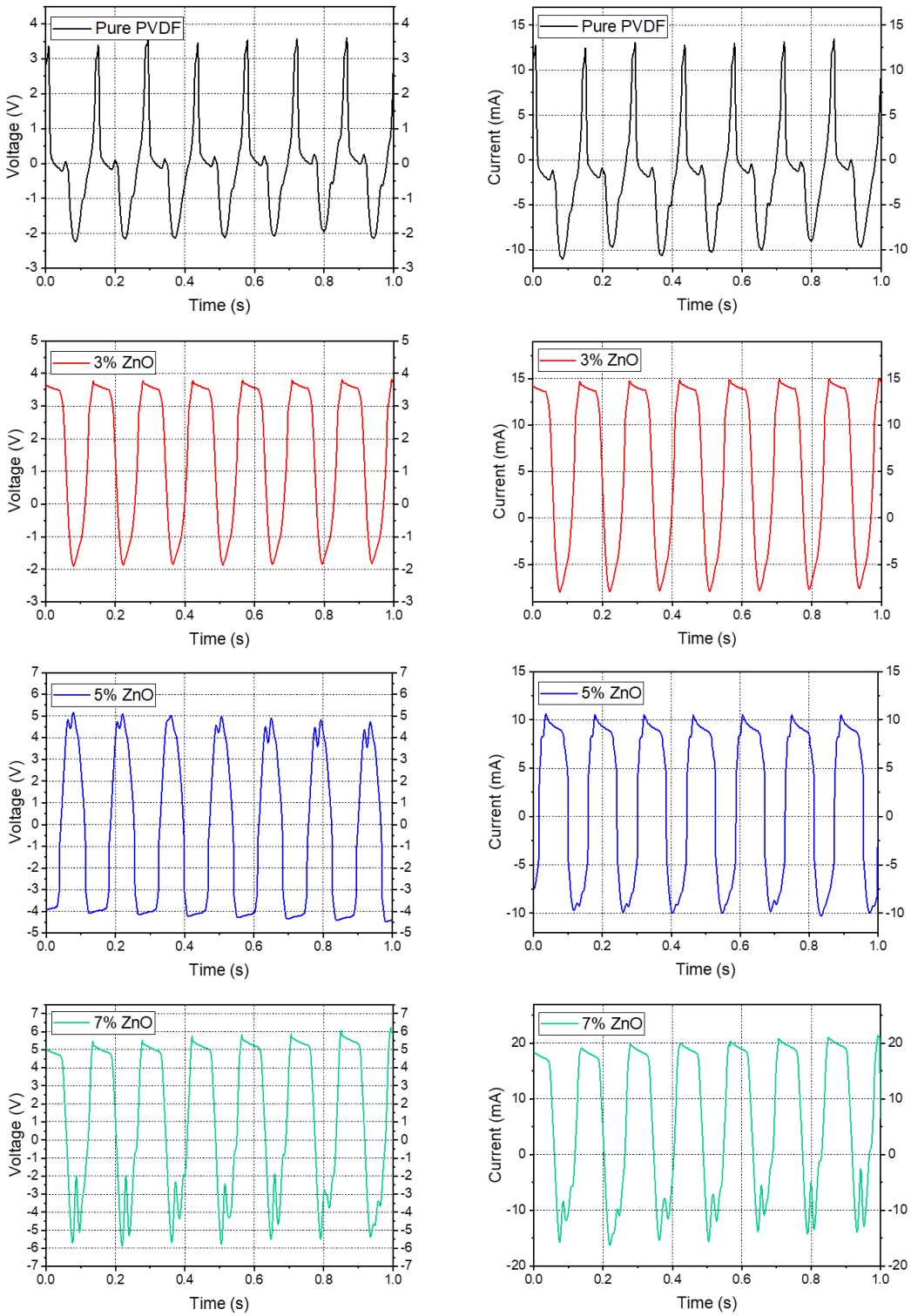

Figure 37. Open-circuit voltage and short-circuit current of poled PVDF thin-film energy harvesters with different ZnO NPs contents.

The measured peak-to-peak V_{oc} data from both unpoled and poled samples are plotted against different ZnO NPs contents in Figure 38. The figure illustrates how the V_{oc} changes after the electrode poling as well as after increasing ZnO NP concentrations in PVDF. These measurements were taken from five different samples for each ZnO NPs content. With the increase of ZnO NPs content, the peak-to-peak V_{oc} increased gradually. The maximum peak-to-peak V_{oc} output of over 11 V was obtained from the poled samples with 7% ZnO NPs content. It can be seen that both integrating the ZnO NPs in PVDF and electrode poling the as-prepared samples have great effects on enhancing the output of thin-film energy harvesters.

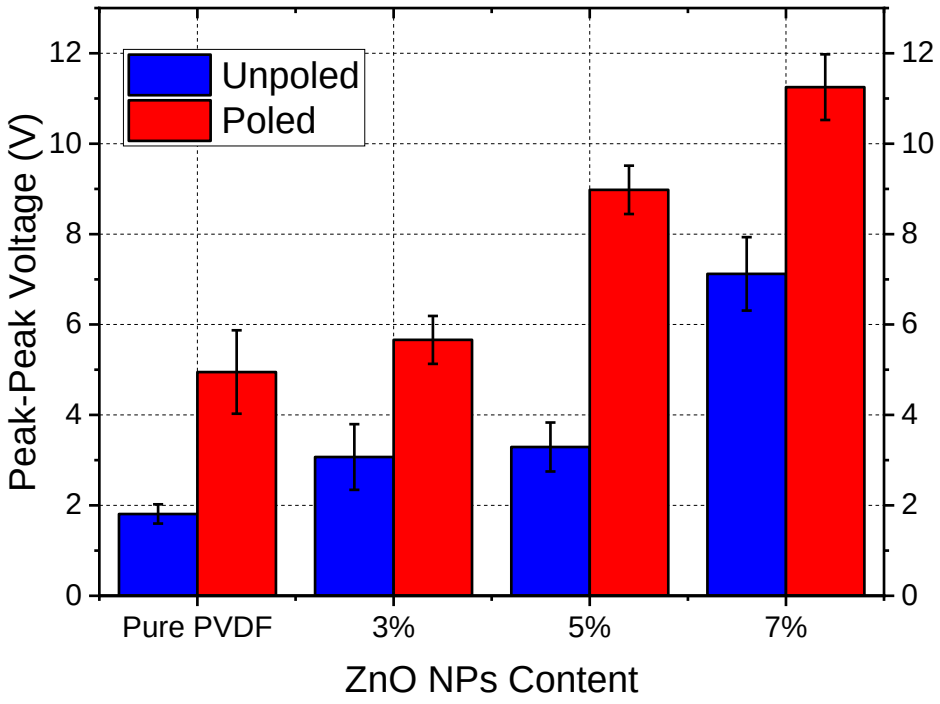

Figure 38. Comparison of peak-to-peak V_{oc} between unpoled and poled PVDF/ZnO thin-film samples for different ZnO NPs contents.

Figure 39 illustrates the peak-to-peak I_{sc} values for different ZnO NPs concentrations before and after the thin-film devices undergo the polarization process. Comparing the results between the poled and unpoled samples showed that the current value of thin-film devices was increased after electrode poling. However, the effect of integrating ZnO NPs at low concentrations (0%, 3%, and 5%) on the current output values is not significant. A slight decrease was observed between the current values of both the unpoled and poled samples when the ZnO NPs concentration was increased from 3% to 5%. The high concentration of ZnO NPs in PVDF at 7% resulted in a significant increase in the current output for both unpoled and poled samples.

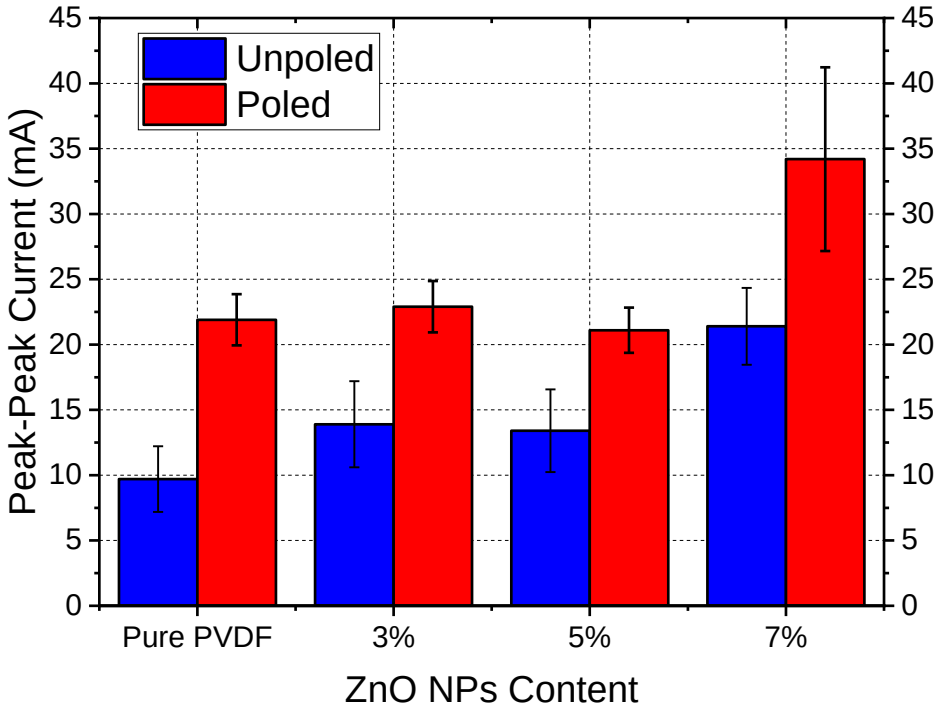

*Figure 39. C*omparison of peak-to-peak I_{sc} between unpoled and poled PVDF/ZnO thin-film samples for different ZnO NPs contents.

Figure 40 illustrates the power output for both the unpoled and poled PVDF/ZnO samples. It shows that increasing the ZnO NPs ratio and poling have positive effects on the output power. Oftentimes, energy harvesters produce AC voltage because most of the testing setups are used to exhibit simple harmonic motion at a constant frequency. Therefore, before calculating the power produced by the thin-film energy harvesters, root mean squares (rms) values for both voltage and current are calculated by the equations:

$$Vrms = \frac{Vp-p}{2\sqrt{2}} \quad (3)$$

$$Irms = \frac{Ip-p}{2\sqrt{2}} \quad (4)$$

$\boldsymbol{V_{rms}}$**:** The root-mean-square or effective value of voltage

$\boldsymbol{I_{rms}}$**:** The root-mean-square or effective value of current

$\boldsymbol{V_{p\text{-}p}}$**:** The voltage value between positive and negative peaks

$\boldsymbol{I_{p\text{-}p}}$**:** The current value between positive and negative peaks

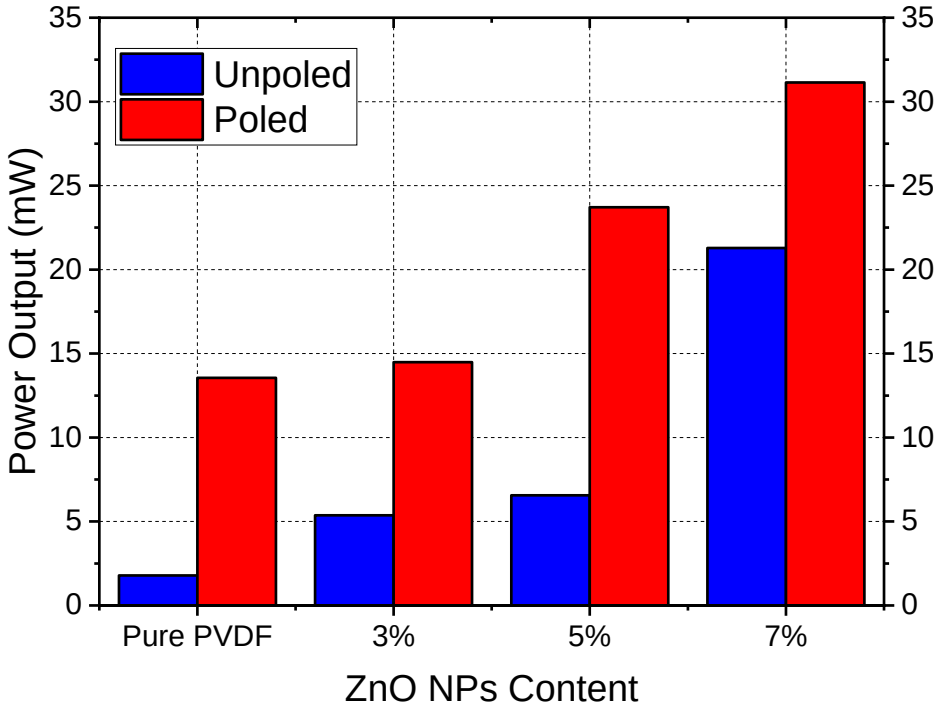

Figure 40. Power output comparison between unpoled and poled PVDF/ZnO thin-film samples for different ZnO NPs contents.

Table 7 shows the overall impact of electrode poling and embedding different amounts of ZnO NPs into PVDF on electrical properties of polymer based thin-film energy harvesters. The power output of the thin-film samples showed continuous improvement as the ZnO NP concentration increases. The comparison shows that thin-film energy harvesters made with higher ZnO NPs exhibited higher effective power output despite the slight decrease in certain current values. Moreover, the thin-film energy harvesters tested after the polarization showed higher power output than the thin-film energy harvesters tested before the polarization process. These results show that the energy harvesting performance of the piezoelectric polymer PVDF can be enhanced by embedding piezoelectric nanoparticles, such as the ZnO NPs, and electrode poling to

polarize the polymer/composites. High-performance energy nanogenerators can potentially be fabricated from these new polymer nanocomposites.

Table 7

Effect of electrode poling on PVDF thin-film energy harvesters

	Pure PVDF	3%	5%	7%
Unpoled peak-peak ~V_{oc} (V)	1.8	3	3.2	7
Unpoled peak-peak ~I_{sc} (mA)	9.7	13.9	13.4	21.4
Unpoled power output (mW)	1.79	5.37	6.56	21.29
Poled peak-peak ~V_{oc} (V)	5	5.7	9	11.2
Poled peak-peak ~I_{sc} (mA)	21.9	22.9	21.1	34.2
Poled power output (mW)	13.55	14.49	23.71	31.14

Table 8 shows the required energy of different macro- and micro-electronic devices, such as microchips, implantable medical devices, and IR sensors, at different power scales. The electrical testing results show that our thin-film energy harvesters are promising to make these devices self-powered in the future.

Table 8

The required energy of different macro- and micro-electronic devices

Device	**The Required Energy**
Microchips	10 mW (10^{-3})
Implantable Medical Devices	10 µW (10^{-6})
IR Sensors	10 nW (10^{-9})

Table 9 shows the output performances of published studies in this field. The output voltage and current values were used for comparison. It can be seen that our samples, especially the poled PVDF thin-film sample with 7% ZnO NPs, provided non-negligible results and improvement.

Table 9

Comparison between this research and some of the other published studies

Ref.	Polymer	Nano Material	Fabrication Method	Poling Technique	Nano Material Content	Output			
						Peak-to-Peak Voltage (V)		Peak-to-Peak Current (mA)	
						Before Poling	After Poling	Before Poling	After Poling
[43]	PVDF-TrFE	ZnO (30 ± 10 nm)	Spin Coating	-	Pure	~2	-	-	-
					1.5%	~3	-	-	-
					4.5%	~3.5	-	-	-
					7.5%	~8.5	-	-	-
					10.5%	~4.5	-	-	-
					12.5%	~5	-	-	-
[71]	PVDF	ZnO	Electrospinning	-	Pure	0.315	-	-	-
					7%	0.62	-	-	-
					15%	1.11	-	-	-
[98]	PVDF	ZnO	Drop Casted	-	Pure	~1	-	-	-
					5%	~1.5	-	-	-
					10%	~2	-	-	-
					15%	~2.5	-	-	-
[99]	PVDF-TrFE	BaTiO3	Spin Coating	Electrode	40%	6	19.6	7.4E-04	1.4E-03
[100]	PVDF	ZnO	Solution Casting and Acid	Corona	50%	-	22	-	9.4E-02
This Study	PVDF	ZnO (20 nm)	Spin Coating	Electrode	Pure	1.8	5	9.7	21.9
					3%	3	5.7	13.9	22.9
					5%	3.2	9	13.4	21.1
					7%	7	11.2	21.4	34.2

Chapter 5

Conclusions and Future Works

5.1 Conclusions

This work investigated the effect of embedding various ratios of ZnO NPs on electrical and mechanical properties of PVDF thin-film energy harvesters as well as the effect of electrode poling on their electrical output. Pristine PVDF and PVDF/ZnO thin-film energy harvesting samples were successfully generated by implementing 3%, 5%, and 7% ZnO NPs into the PVDF. DMF was used to dissolve the PVDF powder and spin coating was used for fabricating the samples. Adding MEK as an additional solvent and using a sonication bath were used to help disperse ZnO NPs in PVDF to achieve a uniform solution. Moreover, using a mixed MEK/DMF solvent in material preparation resulted in less rigid thin-film samples than using only DMF as the sole solvent.

Tensile testing was used to measure the mechanical properties of the samples. The results show that the pure PDVF, as well as samples with 3% and 5% ZnO NP concentrations, had comparable Young's Modulus values at 1257.22 MPa, 1334.92. Mpa, and 1284.58 MPa, respectively. The PVDF thin-film samples with 7% ZnO NPs had the lowest Young's Modulus at 994.21 MPa. Because Young's modulus is the indication of stiffness, the 7% PVDF/ZnO samples with the lowest Young's modulus can be a promising material as energy harvesters where relatively small mechanical forces can be used to deform the devices.

The electrical testing results showed that both the voltage and the power output increased as a function of ZnO NPs concentration. Among the unpoled samples, the highest peak-to-peak voltage output of 7 V was produced by the PVDF thin-film energy

harvester with 7% ZnO NPs, which was approximately four times higher than the output voltage of the unpoled pure PVDF sample. Moreover, the highest power output for unpoled samples was produced by PVDF thin-film energy harvester with 7% ZnO NPs at 21.29 mW. Another technique used to improve the electrical output of energy harvesters was electrode poling. After the electrode poling process, significant enhancement was observed from all tested samples. The poled 5% PVDF/ZnO sample had the maximum enhancement by 181% whereas the poled 7% PVDF/ZnO sample had the minimum enhancement by 60%. However, the poled 7% PVDF/ZnO sample had the highest peak-to-peak V_{oc} and power values at 11.2 V and 31.14 mW, respectively, after polarization.

Particularly, our study demonstrates that the voltage and power output of thin-film PVDF devices can be improved by embedding ZnO NPs and using electrode poling technique. These thin-film PVDF/ZnO NP energy harvesters are promising candidates for portable macro- and micro-electronic devices.

5.2 Future Works

There are several possible aspects from this study worth further investigation in the future. The potential outcomes from these activities could improve the performance of the energy harvesters:

- Continuous technical improvements. While working on the recipe, adding different amounts of ZnO NPs into the solution was explored. It appeared that adding more than 7% ZnO NPs (0.07 g) and having the uniform solution was challenging using the current solvents. According to our data, higher ZnO NP concentration in PVDF results in higher electrical output fro the sample. Therefore, future research could involve a recipe for integrating more ZnO NPs in

PVDF. This will help future researchers to investigate the effect of adding more ZnO NPs on both mechanical and electrical properties of the thin-film energy harvesters. Moreover, since we used nanoparticles in this research, their sizeand properties have drastical effectson the final material. Therefore, investigating different sizes of ZnO NPs could help improve the mechanical properties of thin-film energy harvesters as well as their mechanical properties. On the other hand, many different nanomaterials can be used as fillers instead of ZnO NPs. Investigating another nanomaterial could help enhance the mechanical and electrical properties of thin-film energy harvesters. In addition, keeping the temperature of each step is important because the temperature of each step affects the piezoelectric properties of the materials which were used in this study. Hence, keeping the temperature of the sonication process could help improve the piezoelectric properties of the devices. Also, developing a low-power electronic device that can be powered by the polymer based thin-film energy harvesters is of importance. Such an experiment will show that our thin-film energy harvesters can be used in real-life practical applications. Moreover, the measurement results on the thin-film samples after polarization were promising. However, due to limited time in our research, the polarization time was limited to 40 minutes for each sample. Extending the polarization time during the electrode poling could potentially enhance the number of dipoles that are aligned, which would positively affect the electrical output of our devices.

- Improvements on data collection. There are other types of techniques that can be used in this study for data collection, which will help evaluate the enhancement of

our thin-film energy harvesters. For instance, measuring the charge capacity, collecting data using the Fourier-transform infrared spectroscopy (FTIR), and imaging the composites with scanning electron microscopy (SEM) can further our understanding of the materials and devices. In order to evaluate the energy generating capacity of piezoelectric polymer composites, using them to charge a capacitor with a proper circuit would show the efficiency and usability of our devices. The data from the FTIR would help investigate how the β-phases change in the PVDF after increasing the ZnO NP concentrations and polarizing the samples. In addition, the SEM can be used to closely inspect the quality of the composites in terms of nanoparticle distribution and allogromation, which are critical factors that can affect the performance of the resulting devices.

- Major future research studies. After the discovery of the triboelectric effect in nanogenerators in 2012, it has been reported that the two effects, triboelectricity and piezoelectricity, both play critical roles in energy harvesters. Consequently, it is possible that our results contain triboelectric charges as well as piezoelectric charges. Therefore, having a different electrical testing setup would help distinguish the contributions of piezoelectric and triboelectric charges from the electro-mechanical measurement. This would help quantify the actual piezoelectric effect of the PVDF thin-film energy harvesters. Also, it would help the investigation on the overall charge capacity of PVDF thin-film energy harvesters from both triboelectricity and piezoelectricity. Another major future study could be the comparative study between PVDF and another polymer. This could help evaluate the performance of PVDF comparing to other polymers. The

last but not the least, investigating how to escalate the manufacturing process is important because, during this research, we obtained about five samples in size of 2.5 cm × 2.5 cm from one batch which took approximately six hours. Another important point about the manufacturing process of these devices is that having a manufacturing technique, such as roll-to-roll processing, that could scale up the production and make it possible to provide larger thin-film energy harvesters for practical applications.

References

[1] H. Liu, J. Zhong, C. Lee, S.-W. Lee, and L. J. A. P. R. Lin, "A comprehensive review on piezoelectric energy harvesting technology: Materials, mechanisms, and applications," *Applied Physics Reviews,* vol. 5, no. 4, p. 041306, 2018.

[2] H. A. I. Sodano, Daniel J Park, Gyuhae, "Comparison of piezoelectric energy harvesting devices for recharging batteries," *Journal of intelligent material systems and structures,* vol. 16, no. 10, pp. 799-807, 2005.

[3] D. Hu, M. Yao, Y. Fan, C. Ma, M. Fan, and M. Liu, "Strategies to achieve high performance piezoelectric nanogenerators," *Nano Energy,* vol. 55, pp. 288-304, 2019.

[4] Z. Yang, S. Zhou, J. Zu, and D. J. J. Inman, "High-performance piezoelectric energy harvesters and their applications," *Joule,* vol. 2, no. 4, pp. 642-697, 2018.

[5] M. Prauzek, J. Konecny, M. Borova, K. Janosova, J. Hlavica, and P. Musilek, "Energy Harvesting Sources, Storage Devices and System Topologies for Environmental Wireless Sensor Networks: A Review," *Sensors,* vol. 18, no. 8, p. 2446, Jul 27 2018, doi: 10.3390/s18082446.

[6] M. Chetto and A. Queudet, *Energy Autonomy of Real-Time Systems*. Elsevier, 2016.

[7] J. Shao, T. Jiang, W. Tang, X. Chen, L. Xu, and Z. L. Wang, "Structural figure-of-merits of triboelectric nanogenerators at powering loads," *Nano Energy,* vol. 51, pp. 688-697, 2018.

[8] S. Wang, Y. Xie, S. Niu, L. Lin, and Z. L. Wang, "Freestanding triboelectric-layer-based nanogenerators for harvesting energy from a moving object or human motion in contact and non-contact modes," *Advanced materials,* vol. 26, no. 18, pp. 2818-2824, 2014.

[9] F.-R. Fan, Z.-Q. Tian, and Z. L. Wang, "Flexible triboelectric generator," *Nano energy,* vol. 1, no. 2, pp. 328-334, 2012.

[10] T. Cheng, Q. Gao, and Z. L. Wang, "The Current Development and Future Outlook of Triboelectric Nanogenerators: A Survey of Literature," *Advanced Materials Technologies,* vol. 4, no. 3, p. 1800588, 2019.

[11] Z. L. Wang, J. Chen, and L. Lin, "Progress in triboelectric nanogenerators as a new energy technology and self-powered sensors," *Energy & Environmental Science,* vol. 8, no. 8, pp. 2250-2282, 2015.

[12] Z. L. Wang, "Triboelectric nanogenerators as new energy technology and self-powered sensors–Principles, problems and perspectives," *Faraday discussions,* vol. 176, pp. 447-458, 2015.

[13] M. Babar, A. Rahman, F. Arif, G. J. S. C. I. Jeon, and Systems, "Energy-harvesting based on internet of things and big data analytics for smart health monitoring," *Sustainable Computing: Informatics and Systems,* vol. 20, pp. 155-164, 2018.

[14] S. Katzir, "Measuring constants of nature: confirmation and determination in piezoelectricity," *Studies in History Philosophy of Science Part B: Studies in History Philosophy of Modern Physics,* vol. 34, no. 4, pp. 579-606, 2003.

[15] S. Mishra, L. Unnikrishnan, S. K. Nayak, and S. Mohanty, "Advances in piezoelectric polymer composites for energy harvesting applications: a systematic review," *Macromolecular Materials Engineering,* vol. 304, no. 1, p. 1800463, 2019.

[16] H. Kim, S. Priya, H. Stephanou, and K. Uchino, "Consideration of impedance matching techniques for efficient piezoelectric energy harvesting," *IEEE transactions on ultrasonics, ferroelectrics, frequency control,* vol. 54, no. 9, pp. 1851-1859, 2007.

[17] S. Priya *et al.*, "A review on piezoelectric energy harvesting: materials, methods, and circuits," *Energy Harvesting Systems,* vol. 4, no. 1, pp. 3-39, 2017.

[18] G. H. Haertling, "Ferroelectric ceramics: history and technology," *Journal of the American Ceramic Society,* vol. 82, no. 4, pp. 797-818, 1999.

[19] K. W. Yoon, J.-H. Kim, and S. J. Kim, "Anisotropic effects of polyvinylidene fluoride on the control of transmitted sound fields through a composite plate," *Smart Materials and Structures,* vol. 7, no. 6, p. 885, 1998.

[20] S.-B. Kim, H. Park, S.-H. Kim, H. C. Wikle, J.-H. Park, and D.-J. Kim, "Comparison of MEMS PZT cantilevers based on d_{31} and d_{33} modes for vibration energy harvesting," *Journal of microelectromechanical systems,* vol. 22, no. 1, pp. 26-33, 2012.

[21] S. Xu, G. Poirier, and N. Yao, "PMN-PT nanowires with a very high piezoelectric constant," *Nano letters,* vol. 12, no. 5, pp. 2238-2242, 2012.

[22] S. Pramanik, B. Pingguan-Murphy, and N. A. Osman, "Developments of immobilized surface modified piezoelectric crystal biosensors for advanced applications," *Int. J. Electrochem. Sci,* vol. 8, pp. 8863-8892, 2013.

[23] T. Jordan and Z. Ounaies, "Piezoelectric ceramics characterization," INSTITUTE FOR COMPUTER APPLICATIONS IN SCIENCE AND ENGINEERING HAMPTON VA, 2001.

[24] J. Valasek, "Piezo-electric and allied phenomena in Rochelle salt," *Physical review,* vol. 17, no. 4, p. 475, 1921.

[25] A. S. Rana and S. Srivastava, "Electricity Generation through Human Power via Piezoelectric Effect," *ESSENCE Int. J. Env. Rehab. Conserv. IX,* pp. 23-27, 2018.

[26] R. Kell, "Modern applications of ferroelectricity," *British Journal of Applied Physics,* vol. 14, no. 5, p. 249, 1963.

[27] E. Aksel and J. L. Jones, "Advances in lead-free piezoelectric materials for sensors and actuators," *Sensors,* vol. 10, no. 3, pp. 1935-1954, 2010.

[28] V. Corral-Flores and D. Bueno-Baqués, "Flexible ferroelectric BaTiO3–PVDF nanocomposites," *Ferroelectrics–Material Aspects,* 2011.

[29] K. Sappati and S. Bhadra, "Piezoelectric polymer and paper substrates: A review," *Sensors,* vol. 18, no. 11, p. 3605, 2018.

[30] B. Sahoo and P. K. Panda, "Dielectric, ferroelectric and piezoelectric properties of (1− x)[Pb 0.91 La 0.09 (Zr 0.60 Ti 0.40) O 3]–x [Pb (Mg 1/3 Nb 2/3) O 3], 0≤ x≤ 1," *Journal of materials science,* vol. 42, no. 12, pp. 4270-4275, 2007.

[31] B. G. Baraskar, P. S. Kadhane, T. C. Darvade, A. R. James, and R. C. Kambale, "BaTiO3-Based Lead-Free Electroceramics with Their Ferroelectric and Piezoelectric Properties Tuned by Ca2+, Sn4+ and Zr4+ Substitution Useful for Electrostrictive Device Application," *Ferroelectrics Their Applications,* p. 113, 2018.

[32] P. Lu, H. Li, Y.-M. Wang, S. Sun, and B. Tuttle, "Growth characteristics of ferroelectric PbTiO3 (PT) and Pb (ZrxTi1− x) O3 thin films by novel single-solid-source metalorganic chemical vapor processing," *Journal of crystal growth,* vol. 181, no. 4, pp. 374-381, 1997.

[33] R. Thielsch, W. Haessler, and W. Brueckner, "Electrical properties and mechanical stress of thick plasma-sprayed Pb (Zr0. 58Ti0. 42) O3 coatings," *Physica status solidi,* vol. 156, no. 1, pp. 199-207, 1996.

[34] D. Van den Ende, P. De Almeida, and S. Van der Zwaag, "Piezoelectric and mechanical properties of novel composites of PZT and a liquid crystalline thermosetting resin," *Journal of materials science,* vol. 42, no. 15, pp. 6417-6425, 2007.

[35] M. Adamczyk, L. Kozielski, A. Lisińska-Czekaj, and D. Czekaj, "Application of the FITSC method for characterization of PZT-type ceramics with the diffuse phase transition," *Journal of Alloys Compounds,* vol. 509, no. 22, pp. 6452-6456, 2011.

[36] W. Zhou and B. Chu, "Strong electromechanical response in lead zirconate titanate metamaterials," *Journal of the American Ceramic Society,* vol. 99, no. 10, pp. 3317-3324, 2016.

[37] W. Hu, "Experimental search for high Curie temperature piezoelectric ceramics with combinatorial approaches," 2011.

[38] J. Chen, X. Tan, W. Jo, and J. Rödel, "Temperature dependence of piezoelectric properties of high-TC Bi (Mg 1/2 Ti 1/2) O 3–PbTiO 3," *Journal of Applied Physics,* vol. 106, no. 3, p. 034109, 2009.

[39] C. K. Jeong *et al.*, "Comprehensive biocompatibility of nontoxic and high-output flexible energy harvester using lead-free piezoceramic thin film," *Apl Materials,* vol. 5, no. 7, p. 074102, 2017.

[40] M. D. Maeder, D. Damjanovic, and N. Setter, "Lead Free Piezoelectric Materials," *Journal of Electroceramics,* vol. 13, no. 1, pp. 385-392, July 01 2004, doi: 10.1007/s10832-004-5130-y.

[41] M. Acosta *et al.*, "BaTiO3-based piezoelectrics: Fundamentals, current status, and perspectives," *Applied Physics Reviews,* vol. 4, no. 4, p. 041305, 2017.

[42] J. Gao, D. Xue, W. Liu, C. Zhou, and X. Ren, "Recent progress on BaTiO3-based piezoelectric ceramics for actuator applications," in *Actuators*, 2017, vol. 6, no. 3: Multidisciplinary Digital Publishing Institute, p. 24.

[43] J. Han, D. Li, C. Zhao, X. Wang, J. Li, and X. Wu, "Highly sensitive impact sensor based on PVDF-TrFE/Nano-ZnO composite thin film," *Sensors,* vol. 19, no. 4, p. 830, 2019.

[44] J. Li, C. Zhao, K. Xia, X. Liu, D. Li, and J. Han, "Enhanced piezoelectric output of the PVDF-TrFE/ZnO flexible piezoelectric nanogenerator by surface modification," *Applied Surface Science,* vol. 463, pp. 626-634, 2019.

[45] Y. Qi and M. C. McAlpine, "Nanotechnology-enabled flexible and biocompatible energy harvesting," *Energy Environmental Science,* vol. 3, no. 9, pp. 1275-1285, 2010.

[46] D. M. Bushnell, Ounaies, Z., and Harrison, J. S., "Piezoelectric Polymers - NASA/CR-2001-211422. N.p., 2001. Web."

[47] K. S. Ramadan, D. Sameoto, and S. Evoy, "A review of piezoelectric polymers as functional materials for electromechanical transducers," *Smart Materials and Structures,* vol. 23, no. 3, p. 033001, 2014.

[48] O. Hamdi, F. Mighri, and D. Rodrigue, "Piezoelectric cellular polymer films: Fabrication, properties and applications," *AIMS Materials Science 5: 845,* vol. 869, 2018.

[49] C. Bowen, "Ferroelectret materials and devices for energy harvesting applications," 2019.

[50] C. Baur, D. J. Apo, D. Maurya, S. Priya, and W. Voit, "Advances in piezoelectric polymer composites for vibrational energy harvesting," in *Polymer composites for energy harvesting, conversion, and storage*: ACS Publications, 2014, pp. 1-27.

[51] H. Kawai, "The piezoelectricity of poly (vinylidene fluoride)," *Japanese journal of applied physics,* vol. 8, no. 7, p. 975, 1969.

[52] G. Gutiérrez-Sánchez, J. Hernando-García, V. Ruiz-Diez, O. Dura, M. L. de la Torre, and J. Sánchez-Rojas, "Comparative assessment of PVDF and PVDF-TrFE piezoelectric polymers for flexible actuators applications," in *Smart Sensors, Actuators, and MEMS VIII*, 2017, vol. 10246: International Society for Optics and Photonics, p. 102460N.

[53] S. Lang and S. Muensit, "Review of some lesser-known applications of piezoelectric and pyroelectric polymers," *Applied Physics A,* vol. 85, no. 2, pp. 125-134, 2006.

[54] N. A. Shepelin *et al.*, "New developments in composites, copolymer technologies and processing techniques for flexible fluoropolymer piezoelectric generators for efficient energy harvesting," *Energy Environmental Science,* vol. 12, no. 4, pp. 1143-1176, 2019.

[55] J. Nunes-Pereira *et al.*, "Poly (vinylidene fluoride) and copolymers as porous membranes for tissue engineering applications," *Polymer Testing,* vol. 44, pp. 234-241, 2015.

[56] L. Ruan, X. Yao, Y. Chang, L. Zhou, G. Qin, and X. Zhang, "Properties and Applications of the β Phase Poly (vinylidene fluoride)," *Polymers,* vol. 10, no. 3, p. 228, 2018.

[57] M. Kim, Y. Wu, E. Kan, and J. Fan, "Breathable and flexible piezoelectric ZnO@ PVDF fibrous nanogenerator for wearable applications," *Polymers,* vol. 10, no. 7, p. 745, 2018.

[58] P. Martins, A. Lopes, and S. Lanceros-Mendez, "Electroactive phases of poly (vinylidene fluoride): Determination, processing and applications," *Progress in polymer science,* vol. 39, no. 4, pp. 683-706, 2014.

[59] D. L. Chinaglia *et al.*, "Influence of the solvent evaporation rate on the crystalline phases of solution-cast poly (vinylidene fluoride) films," *Journal of applied polymer science,* vol. 116, no. 2, pp. 785-791, 2010.

[60] X. Wang, F. Sun, G. Yin, Y. Wang, B. Liu, and M. Dong, "Tactile-sensing based on flexible PVDF nanofibers via electrospinning: a review," *Sensors,* vol. 18, no. 2, p. 330, 2018.

[61] D. M. Esterly, "Manufacturing of Poly (vinylidene fluoride) and Evaluation of its Mechanical Properties," Doctoral dissertation, Virginia Tech, 2002.

[62] B. Lin and V. Giurgiutiu, "Modeling and testing of PZT and PVDF piezoelectric wafer active sensors," *Smart Materials Structures,* vol. 15, no. 4, p. 1085, 2006.

[63] S. Crossley, R. Whiter, and S. Kar-Narayan, "Polymer-based nanopiezoelectric generators for energy harvesting applications," *Materials Science Technology,* vol. 30, no. 13, pp. 1613-1624, 2014.

[64] W. Xia, Z. Xu, Z. Zhang, and H. Li, "Dielectric, piezoelectric and ferroelectric properties of a poly (vinylidene fluoride-co-trifluoroethylene) synthesized via a hydrogenation process," *Polymer,* vol. 54, no. 1, pp. 440-446, 2013.

[65] W. Xia, Y. Gu, C. You, C. Cao, Z. Xu, and Z. Zhang, "A crystal phase transition and its effect on the dielectric properties of a hydrogenated P (VDF-co-TrFE) with low TrFE molar content," *RSC Advances,* vol. 5, no. 130, pp. 107557-107565, 2015.

[66] R. Mohd Dahan, A. N. Arshad, M. H. Md Razif, N. S. Mahmud Zohdi, and M. R. Mahmood, "Structural and electrical properties of PVDF-TrFE/ZnO bilayer and filled PVDF-TrFE/ZnO single layer nanocomposite films," *Advances in Materials Processing Technologies,* vol. 3, no. 3, pp. 300-307, 2017.

[67] H. Xu, Z.-Y. Cheng, D. Olson, T. Mai, Q. Zhang, and G. Kavarnos, "Ferroelectric and electromechanical properties of poly (vinylidene-fluoride–trifluoroethylene–chlorotrifluoroethylene) terpolymer," *Applied Physics Letters,* vol. 78, no. 16, pp. 2360-2362, 2001.

[68] P. I. Devi and K. Ramachandran, "Dielectric studies on hybridised PVDF–ZnO nanocomposites," *Journal of Experimental Nanoscience,* vol. 6, no. 3, pp. 281-293, 2011.

[69] Z. Li, X. Zhang, and G. Li, "In situ ZnO nanowire growth to promote the PVDF piezo phase and the ZnO–PVDF hybrid self-rectified nanogenerator as a touch sensor," *Physical Chemistry Chemical Physics,* vol. 16, no. 12, pp. 5475-5479, 2014.

[70] J. S. Dodds, F. N. Meyers, and K. J. Loh, "Piezoelectric characterization of PVDF-TrFE thin films enhanced with ZnO nanoparticles," *IEEE Sensors Journal,* vol. 12, no. 6, pp. 1889-1890, 2011.

[71] M. S. S. Bafqi, R. Bagherzadeh, and M. Latifi, "Fabrication of composite PVDF-ZnO nanofiber mats by electrospinning for energy scavenging application with enhanced efficiency," *Journal of Polymer Research,* vol. 22, no. 7, p. 130, 2015.

[72] A. Hartono, Darwin, Ramli, S. Satira, M. Djamal, and Herman, "Electric field poling 2G V/m to improve piezoelectricity of PVDF thin film," in *AIP Conference Proceedings,* 2016, vol. 1719, no. 1: AIP Publishing, p. 030021.

[73] T.-C. Hsu and P. Geil, "Deformation and transformation mechanisms of poly (vinylidene fluoride)(PVF 2)," *Journal of materials science,* vol. 24, no. 4, pp. 1219-1232, 1989.

[74] R. Gregorio and E. Ueno, "Effect of crystalline phase, orientation and temperature on the dielectric properties of poly (vinylidene fluoride)(PVDF)," *Journal of materials science,* vol. 34, no. 18, pp. 4489-4500, 1999.

[75] S. K. Mahadeva, J. Berring, K. Walus, and B. Stoeber, "Effect of poling time and grid voltage on phase transition and piezoelectricity of poly (vinyledene fluoride) thin films using corona poling," *Journal of Physics D: Applied Physics,* vol. 46, no. 28, p. 285305, 2013.

[76] L. Dong *et al.*, "Piezoelectric Buckled Beam Array on a Pacemaker Lead for Energy Harvesting," *Advanced Materials Technologies,* vol. 4, no. 1, p. 1800335, 2019.

[77] E. Nour *et al.*, "Low-frequency self-powered footstep sensor based on ZnO nanowires on paper substrate," *Nanoscale Research Letters,* vol. 11, no. 1, p. 156, 2016.

[78] K. J. Loh and D. Chang, "Zinc oxide nanoparticle-polymeric thin films for dynamic strain sensing," *Journal of Materials Science,* vol. 46, no. 1, pp. 228-237, 2011.

[79] K. S. Siddiqi, A. ur Rahman, and A. Husen, "Properties of zinc oxide nanoparticles and their activity against microbes," *Nanoscale research letters,* vol. 13, no. 1, pp. 1-13, 2018.

[80] R. Araneo *et al.*, "Design concepts, fabrication and advanced characterization methods of innovative piezoelectric sensors based on ZnO nanowires," *Sensors,* vol. 14, no. 12, pp. 23539-23562, 2014.

[81] Y.-C. Hu, W.-L. Hsu, Y.-T. Wang, C.-T. Ho, and P.-Z. Chang, "Enhance the pyroelectricity of polyvinylidene fluoride by graphene-oxide doping," *Sensors,* vol. 14, no. 4, pp. 6877-6890, 2014.

[82] H. Zhu, J. Matsui, S. Yamamoto, T. Miyashita, and M. Mitsuishi, "Solvent-dependent properties of poly (vinylidene fluoride) monolayers at the air–water interface," *Soft Matter,* vol. 11, no. 10, pp. 1962-1972, 2015.

[83] W. Ma, J. Zhang, S. Chen, and X. Wang, "β-Phase of poly (vinylidene fluoride) formation in poly (vinylidene fluoride)/poly (methyl methacrylate) blend from solutions," *Applied surface science,* vol. 254, no. 17, pp. 5635-5642, 2008.

[84] M. Li *et al.*, "Controlling the microstructure of poly (vinylidene-fluoride)(PVDF) thin films for microelectronics," *Journal of Materials Chemistry C,* vol. 1, no. 46, pp. 7695-7702, 2013.

[85] W. Ma, J. Zhang, S. Chen, and X. Wang, "Crystalline phase formation of poly (vinylidene fluoride) from tetrahydrofuran/N, N-dimethylformamide mixed solutions," *Journal of Macromolecular Science®, Part B: Physics,* vol. 47, no. 3, pp. 434-449, 2008.

[86] P. Fakhri *et al.*, "Flexible hybrid structure piezoelectric nanogenerator based on ZnO nanorod/PVDF nanofibers with improved output," *RSC advances,* vol. 9, no. 18, pp. 10117-10123, 2019.

[87] K. Xia, Y.-c. Li, J. Li, B. Xie, C.-m. Zhao, and J. Han, "Research on the effect of spin-coating process on ferroelectric phase of PVDF-TrFE/ZnO film," in *2016 Symposium on Piezoelectricity, Acoustic Waves, and Device Applications (SPAWDA)*, 2016: IEEE, pp. 248-252.

[88] S. CK, U. Valiyaneerilakkal, K. Singh, and S. Varghese, "Device level optimization of poly (vinylidene fluoride-trifluoroethylene)–zinc oxide polymer nanocomposite thin films for ferroelectric applications," *Journal of Applied Physics*, vol. 118, no. 20, p. 204102, 2015.

[89] R. S. Sabry and A. D. Hussein, "Nanogenerator based on nanocomposites PVDF/ZnO with different concentrations," *Materials Research Express*, vol. 6, no. 10, p. 105549, 2019.

[90] P. B. Khoza, M. J. Moloto, and L. M. Sikhwivhilu, "The effect of solvents, acetone, water, and ethanol, on the morphological and optical properties of ZnO nanoparticles prepared by microwave," *Journal of Nanotechnology*, vol. 2012, 2012.

[91] E. Castanet, M. A. Thamish, N. Hameed, A. Krajewski, L. F. Dumée, and K. Magniez, "Zinc Oxide PVDF Nano-Composites–Tuning Interfaces toward Enhanced Mechanical Properties and UV Protection," *Advanced Engineering Materials*, vol. 19, no. 3, p. 1600611, 2017.

[92] R. S. Dahiya, M. Valle, G. Metta, L. Lorenzelli, and S. Pedrotti, "Deposition, processing and characterization of P (VDF-TrFE) thin films for sensing applications," in *SENSORS, 2008 IEEE*, 2008: IEEE, pp. 490-493.

[93] C. Li, P.-M. Wu, S. Lee, A. Gorton, M. J. Schulz, and C. H. Ahn, "Flexible dome and bump shape piezoelectric tactile sensors using PVDF-TrFE copolymer," *Journal of Microelectromechanical Systems*, vol. 17, no. 2, pp. 334-341, 2008.

[94] G. D. Jones *et al.*, "Characterization, performance and optimization of PVDF as a piezoelectric film for advanced space mirror concepts," Sandia National Laboratories, 2005.

[95] C. Wan and C. R. Bowen, "Multiscale-structuring of polyvinylidene fluoride for energy harvesting: the impact of molecular-, micro-and macro-structure," *Journal of Materials Chemistry A*, vol. 5, no. 7, pp. 3091-3128, 2017.

[96] F. Kajzar and J.-M. Nunzi, "Molecule orientation techniques," in *Beam Shaping and Control with Nonlinear Optics*: Springer, 2002, pp. 101-132.

[97] D. Ghosh, S. Bhandari, T. K. Chaki, and D. Khastgir, "Development of a high performance high voltage insulator for power transmission lines from blends of polydimethylsiloxane/ethylene vinyl acetate containing nanosilica," *RSC Advances,* vol. 5, no. 71, pp. 57608-57618, 2015.

[98] H. H. Singh, S. Singh, and N. Khare, "Enhanced β-phase in PVDF polymer nanocomposite and its application for nanogenerator," *Polymers for Advanced Technologies,* vol. 29, no. 1, pp. 143-150, 2018.

[99] S. Siddiqui, D.-I. Kim, M. T. Nguyen, S. Muhammad, W.-S. Yoon, and N.-E. Lee, "High-performance flexible lead-free nanocomposite piezoelectric nanogenerator for biomechanical energy harvesting and storage," *Nano Energy,* vol. 15, pp. 177-185, 2015.

[100] Y. Mao, P. Zhao, G. McConohy, H. Yang, Y. Tong, and X. Wang, "Sponge-like piezoelectric polymer films for scalable and integratable nanogenerators and self-powered electronic systems," *Advanced Energy Materials,* vol. 4, no. 7, p. 1301624, 2014.